Development of an Affordable Tissue Deformation Device for Dynamic Elastography of Bio-Structural Response to Mechanical Load

J.Bonnici, L.Clark, L.Jarvie, E.Quinlan, R.Singh, D.Wilkinson

16TH APRIL 2024

Department of Bioengineering
Imperial College London

A Project Report Submitted in
Partial Fulfilment of the MEng Biomedical Engineering Degree

Supervisors:
Dr Naomi Nakayama
and Sam Mason
n.nakayama@imperial.ac.uk
s.mason22@imperial.ac.uk

Department of Bioengineering

Development of an Affordable Deformation Device

J.Bonnici, L.Clark, L.Jarvie, E.Quinlan, R.Singh, D.Wilkinson

16TH APRIL 2024

WORD COUNT: 4969

ABSTRACT

This project introduces the development of an affordable device compatible with dynamic imaging techniques for characterising the mechanical properties and structural remodelling of biological tissues under external forces. The lack of affordable and accessible devices capable of applying controlled, compressive mechanical deformations has limited the scope of such investigations.

The device was separated into four primary aspects: tissue housing, force application, force sensing and imaging. Two final prototype models were designed using CAD and 3D printed. The calibrated spring prototype, while more cost-effective, encountered challenges in force application due to spring buckling, which restricted its scope for testing and highlighted an area for future improvement. Conversely, the load cell prototype could accurately apply high-resolution, controlled compressive forces. This prototype offered dual operational modes, enabling users to choose between specifying the magnitude of deformation or the applied force. Challenges such as sterility and maintaining sample viability were identified, pointing to areas for future developments.

For proof-of-concept testing, experiments were carried out using cellulose sponge samples. These tests produced force-displacement data from which consistent elastic moduli values were calculated, demonstrating the device's reliability in measuring global mechanical properties. Before moving on to biological tissue testing, further assessment and validation of the device is needed. The device's ability to apply precise mechanical deformations and facilitate observation of resultant anatomical changes presents its potential applications in fields such as sustainable agriculture and diagnostic medicine. Ultimately, this project provides a foundational step towards future advancements in studying tissue mechanics and understanding tissue remodelling processes.

NOMENCLATURE

ACME – Automated Confocal Micro-Extensometer

CAD – Computer Aided Design

DFMEA – Design Failure Mode and Effects Analysis

GM – Genetically Modified

OCT – Optical Coherence Tomography

UI – User Interface

Acclimation – Short term changes of structure in response to stimuli

Elastic Modulus – Resistance to elastic deformation

Hermetic Seal – Airtight seal

1 Introduction

1.1 Project Overview

Understanding the mechanical properties and structural remodelling of biological tissues in response to external forces is important for investigating the fundamental principles of tissue growth, development and acclimation. In particular, the ability to apply precise mechanical deformation to tissues and observe the resultant anatomical changes is useful for studies ranging from plant biomechanics to tissue engineering and regenerative medicine. The lack of affordable and accessible devices capable of applying controlled, compressive mechanical deformations has limited the scope of such investigations.

This project aims to develop an affordable tissue deformation device compatible with non-invasive dynamic imaging techniques to provide real-time insights into tissue responses to mechanical stresses by applying, controlling and quantifying compressive forces and strains. Before advancement can be made to experiments on biological tissues, our project will use a cellulose sponge sample to demonstrate initial proof-of-concept. While the project primarily focuses on plant mechanoresponse, the envisioned device is designed to be universally applicable to a wide spectrum of biological tissues. The goal is to enable researchers to study the mechanical and structural changes in tissues under load, thereby improving understanding of how tissues remodel in response to mechanical stimuli.

1.2 Key Objectives

The project's key objectives were to design and prototype a device which meets the criteria shown in Table 1.

Table 1: Key objectives and descriptions.

Objective	**Description**
Application of a user-specified compressive force or deformation	Enable high resolution application of user-specified forces and deformations.
Application of a sustained force or deformation	Apply a continuous force or deformation over extended periods of 3-14 days, an important feature for studying long-term remodelling of biological tissues.
Compatibility with non-invasive imaging techniques	Allow real-time monitoring of sample response without disrupting its integrity.
Characterisation of global mechanical properties	Facilitate assessment and recording of the stress-strain relationship of the whole sample.
Characterisation of local mechanical properties	Allow detailed study of spatial mechanical properties, e.g. the variation of stress and strain within the sample.
Observation of anatomical changes	Allow monitoring of structures within the sample including pore size, shape and organisation.
Affordability	Minimise cost to ensure accessibility to a wide range of research laboratories.
Reusability	Allow multiple uses without loss of functionality, promoting sustainable research practices.
Low resource intensity	Require minimal equipment and avoid complex setup procedures to further enhance accessibility.
Sterility and sample preservation	Prevent external contaminants from entering the sterile field, an important feature for studying tissue remodelling for 3-14 days.

2 Background

2.1 Tissue Mechanoresponse

Mechanoresponse in biological tissues is a fundamental aspect of the survival and acclimation strategies across all living organisms. Living tissues remodel in response to the mechanical stresses placed on them. For example, Wolff's Law demonstrates that bones continuously remodel in response to applied forces by depositing tissue in areas experiencing high stress and resorbing bone from areas of low stress, maintaining a skeleton that can withstand physical demands more effectively [1].

Similarly, in response to loading, plants undergo thigmomorphogenesis - chemical, genetic and structural alterations that allow plants to acclimate to mechanical stresses in their environment [2]. Kouhen et al. highlight wind-induced sway as the primary mechanical stress in terrestrial plants, triggering an interchanging compressive and tensile force [3]. Additional stresses such as rain and herbivory further complicate the mechanical environment plants must navigate. Over longer periods, structural remodelling in plant stems is observed including secondary xylem development (wood formation) [4] - allowing plants to optimise growth and survival under varying mechanical conditions.

2.2 Applications

In sustainable agriculture, the drive to enhance crop resilience is a key factor in safeguarding food security and economic viability. A significant challenge faced by the industry is lodging – the permanent displacement of plant stems from their vertical position due to mechanical stresses such as wind and rain, leading to severe crop failure. In the UK, lodging inflicts a substantial economic impact, with estimates suggesting losses of up to £120 million annually to the oilseed rape industry alone [5].

Traditional agricultural practices, such as Mugifumi farming, have long utilised stress priming, a method where controlled stress is applied to crops through treading or rolling at a young age to induce tissue remodelling, resulting in plants that are structurally stronger and more resilient to environmental mechanical stresses [6]. Modern approaches are exploring the genetic modification of crops to produce phenotypes that remodel in response to minor loads. The device could provide a means to characterise the mechanical properties and remodelling of plant stems. It would enable precise control over the mechanical environment, allowing researchers to study the effectiveness of stress priming techniques, assess the resilience of GM crops and reduce crop susceptibility to lodging.

In medical diagnostics, the mechanical properties of tissues are valuable biomarkers for various diseases. Diseased tissues often exhibit mechanical properties that differ markedly from their healthy counterparts, observed in conditions including cancer and atherosclerosis, providing a potential diagnostic indicator [7]. Furthermore, in tissue engineering and regenerative medicine the device could assist with research into the design of scaffolds and implants, which must mimic the mechanical environment of the body’s natural tissues [8].

2.3 Existing Devices

In the current landscape, most commercial devices test samples in uniaxial tension such as ACME [9] and ADMET BioTense [10]. Although current devices have furthered understanding of tissue mechanics, given that biological tissues are subjected to both compressive and tensile forces in their natural environments, there is a need for more devices capable of applying compressive loading to reflect this. Table 2 summarises a few existing devices.

Table 2: Summary of existing deformation devices.

Device	Strengths	Weaknesses
ADMET BioTense	▪ High resolution force application (1mN) ▪ Sterilisable	▪ Tensile only ▪ Expensive ▪ Bulky setup (Figure 1) ▪ Only compatible with inverted optical microscopy
ACME	▪ High resolution force application (1mN) ▪ Small and light ▪ Accessible software ▪ Commercially available hardware	▪ Tensile only ▪ Only compatible with confocal microscopy
LINKAM Modular Force Stage [11]	▪ Compressive and tensile loading ▪ High resolution force application (10mN) ▪ Temperature and humidity control	▪ Expensive (£48,000) ▪ Complex operation ▪ Bulky setup
INSTRON 6800 Universal Testing System [12]	▪ Compressive and tensile loading ▪ High data acquisition rate (5KHz) ▪ Industry standard for acquiring mechanical properties	▪ Expensive ▪ Complex operation ▪ Bulky setup ▪ Not compatible with imaging ▪ Difficult for small biological tissue testing

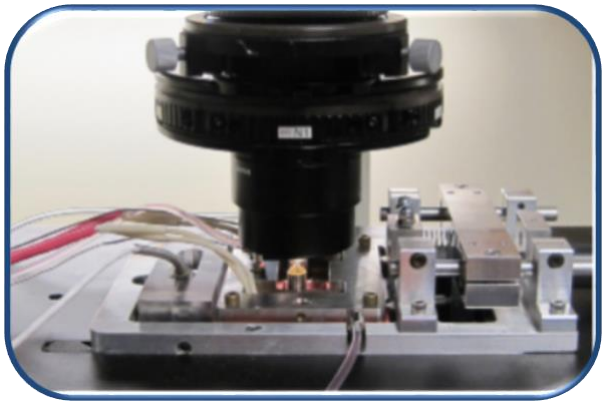

Figure 1: Image of ADMET BioTense atop an inverted microscope [10].

Existing devices share challenges including high costs, operational complexity and limited integration with non-invasive dynamic imaging technologies. Furthermore, the lack of standardised datasets and appropriate instruments for compressive testing of soft tissues impedes advances in mechanobiology and its real-world integration. This gap in the market justifies this project which seeks to leverage the strengths of existing devices while enhancing affordability, reducing resource intensity and increasing compatibility with a range of dynamic imaging technologies.

3 Methods

3.1 Design Overview

The device was broken down into four aspects: tissue housing, force application, force sensing and imaging (Table 3). To assess the effectiveness of design options for each aspect of the device, a decision matrix was created (8.3 Appendix C). Each design option was evaluated and scored across several weighted criteria with the calculated aggregate scores used to inform component selection for prototyping.

Table 3: Intended function of each design aspect.

Design Aspect	**Function**
Tissue housing	Keep sample stationary and sterile under imaging device during testing
Force application	Apply a user-specified force or deformation at high resolution
Force sensing	Accurately sense the applied force and enable feedback to the applicator
Imaging	Obtain high resolution images during testing to enable analysis

3.2 Prototypes

The initial prototype was important for proof-of-concept of the original design ideas and for testing imaging compatibility. The housing was 3D printed and a manually operated bolt applied force to the sample (Figures 2A, 3A). The second prototype (Figures 2B, 3B) incorporated a load cell to provide precise force sensing capability. Finally, the third prototype (Figures 2C, 3C) employed a calibrated spring for force measurement, aiming to increase affordability and simplify the sterilisation process.

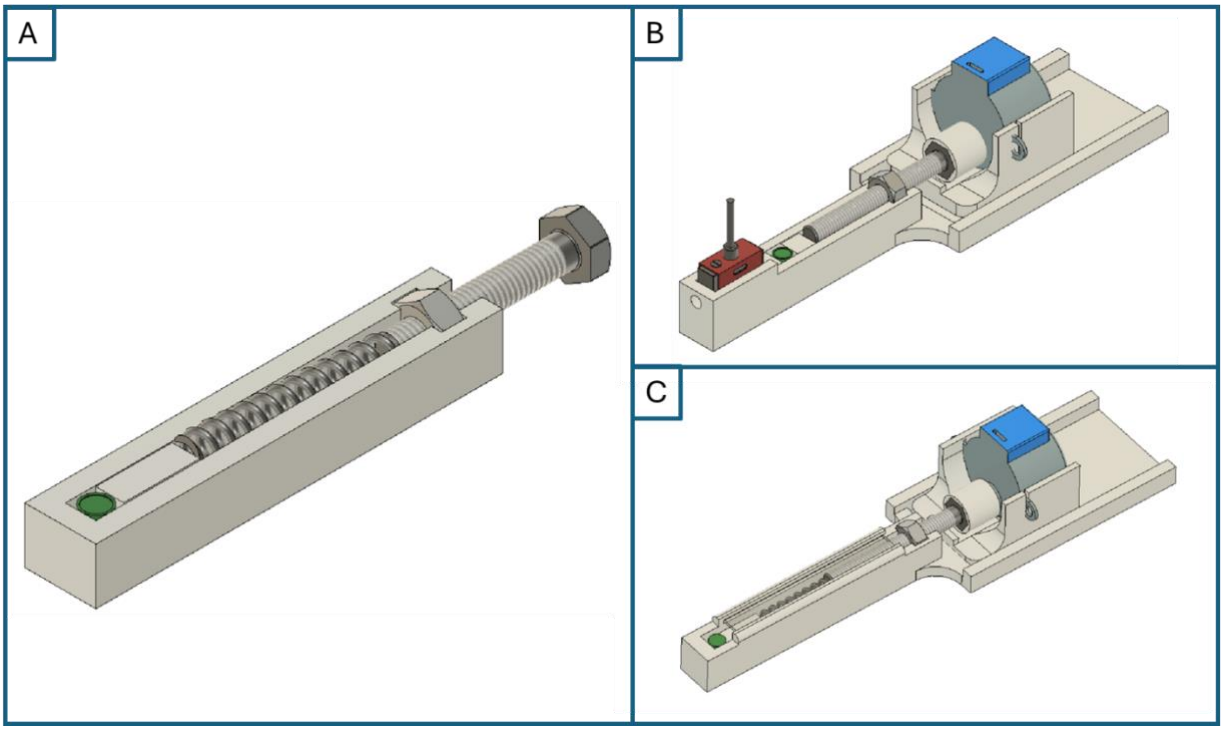

Figure 2: CAD designs of prototypes. (A) Proof-of-concept design. (B) Load cell design. (C) Calibrated spring design.

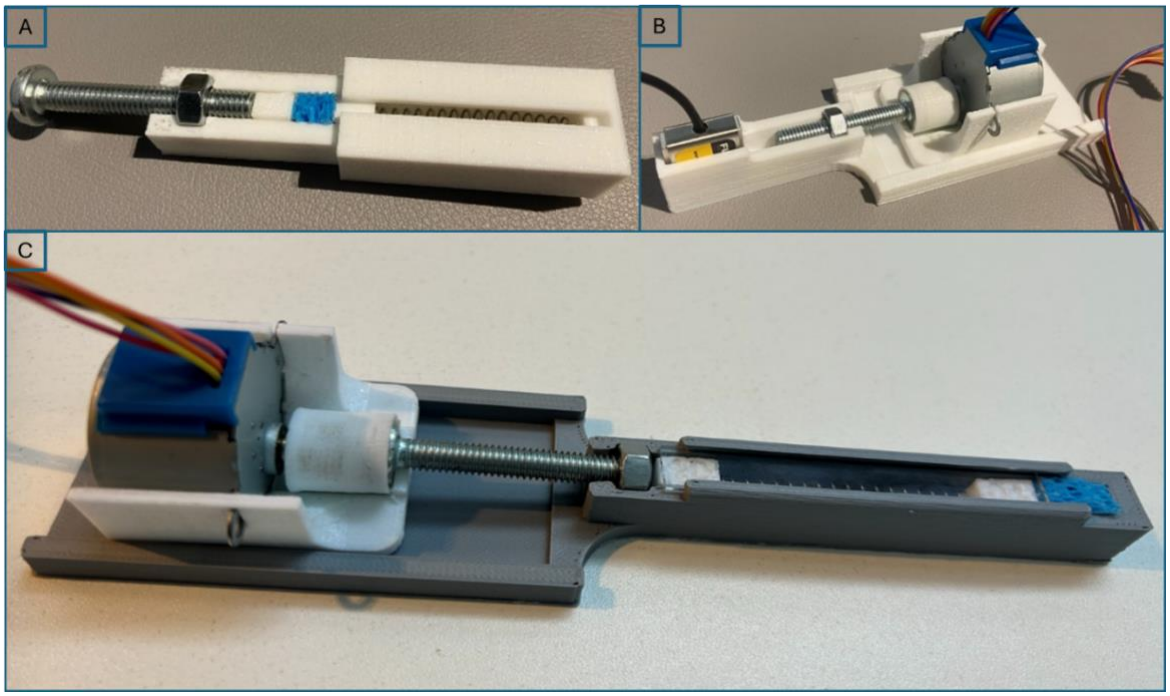

Figure 3: Images of prototypes. (A) Proof-of-concept prototype. The spring is held in with the cover shown. The cover has a small slot cut in it to help visualise the spring and sample (B) Early load cell prototype. (C) Calibrated spring prototype.

3.3 Sample Selection

For testing, a cellulose sponge was selected for its consistent mechanical properties - unlike the variability typically seen in biological samples. Its large and numerous pores were advantageous as they could be analysed more effectively with OCT. The irregularity of these pores provides local variations in the stiffness, reflecting the heterogeneous nature of plant tissue [13]. Additionally, using a cellulose sponge may provide a closer approximation to the mechanical properties of plant tissues (compared to other sponge materials such as polyurethane) since cellulose is the primary component of cell walls in plants [14].

3.4 Housing

Using CAD software and 3D printing, the housing was engineered to secure the sample, force applicator and sensor firmly in place (Appendix E). The decision matrix (Appendix C) identified PLA as the most suitable housing material due to its cost-effectiveness and ease of implementation. The housing design was split into two primary variants: one tailored to integrate with the load cell and another configured for the calibrated spring. Both designs retained core similarities, with slight modifications to accommodate each force sensing modality, easing the continuation of development.

The housing comprises three primary parts (Figure 4): a bolt adapter, the main chamber and a motor enclosure. The bolt adapter connects the stepper motor shaft to the bolt head and can be customised to accommodate a range of bolt sizes. The adapter pushes onto the motor shaft with a friction fit, which transfers rotational movement of the motor to the bolt. The main chamber is further divided into four sections: a track on which the motor enclosure sits to align movement in a single axis, a slot for accommodating the hex-nut, a cradle for the force-sensing element (either a load cell or calibrated spring) and a compartment for the sample. Throughout prototyping, a 40mm M6 bolt was used however the designs can be adjusted to accommodate varying lengths and diameters of bolts and hence different sized samples, increasing versatility. 3D printed rectangular spacer blocks (Figure 5) transmit uniform force to the sample and load cell, increasing the accuracy of the applied and measured force. They also ensure that the sample is protected from the twisting motion of the bolt and the load cell is shielded from direct contact with a wet sample. The motor enclosure twists-and-locks into the main chamber for ease of assembly. It stabilises the motor and locks the bolt and bolt adapter in place. It is positioned on the plate of the main chamber and moves forwards and backwards within raised rails on each side, ensuring controlled linear motion as the bolt screws into the nut.

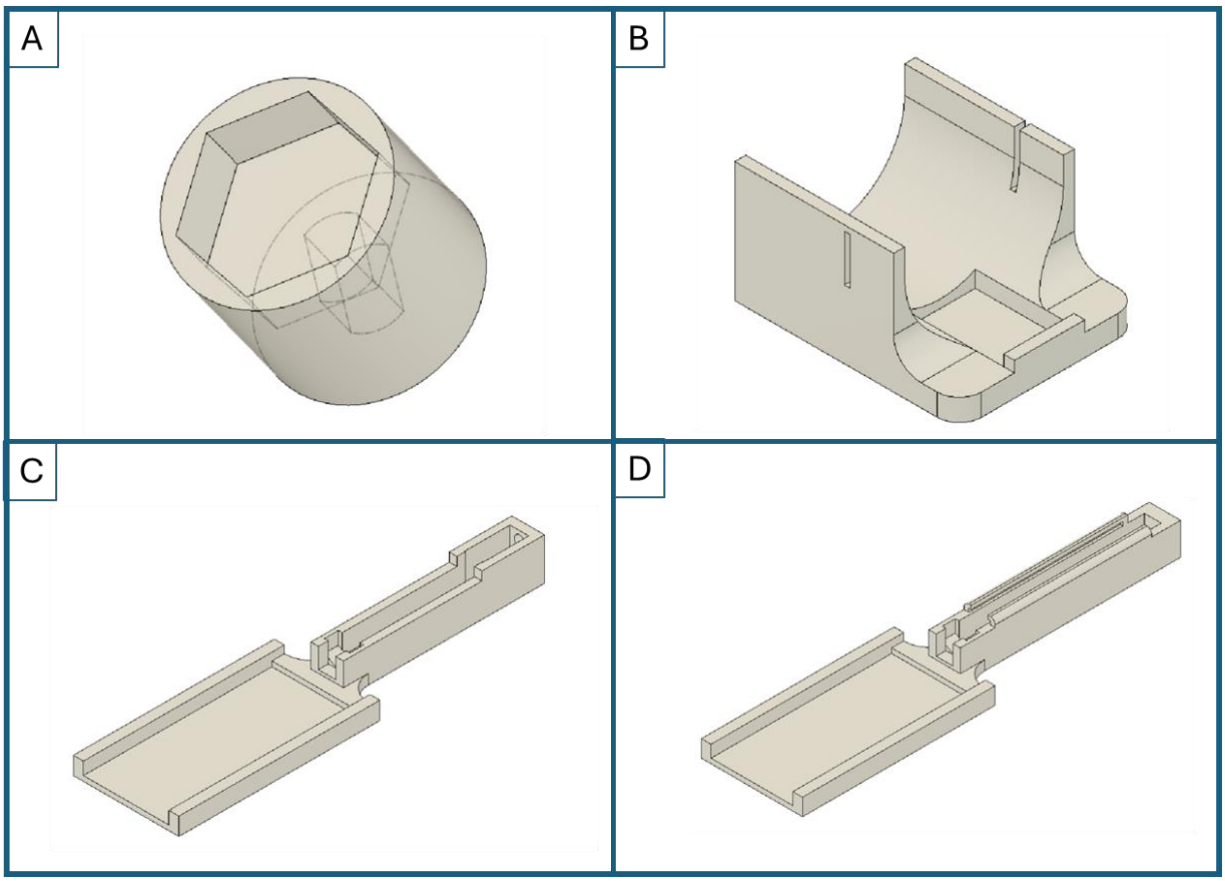

Figure 4: Primary components of housing. (A) Bolt adapter. (B) Motor enclosure. (C) Housing of load cell prototype. (D) Housing of calibrated spring prototype.

Figure 5: Load cell prototype with spacer blocks.

3.5 Force Application

As shown in the Decision Matrix, the highest scoring methods were stepper motors and voice coils, scoring 53 and 50.5 respectively. A voice coil is an electromechanical device made of a conductive coil wound around a magnet and is commonly used in audio and precision motion applications. When current flows through the coil, it experiences a force due to interaction with the magnetic field described by Lorentz's Law [15]. This force is directly proportional to the current and acts on an attached actuator to translate electrical energy into mechanical motion. To evaluate the voice coils, a jig was constructed to position the voice coil above a mass balance to measure the produced force (Figure 6). Although they offered precise and accurate force application, their main drawback was the need for continuous current supply, leading to overheating and lower energy efficiency, making them less suitable than stepper motors for applying force over a long time period. The stepper motor, which converts rotational movement into linear displacement, was tested with a load cell and successfully met the design specifications for force application (Table 3).

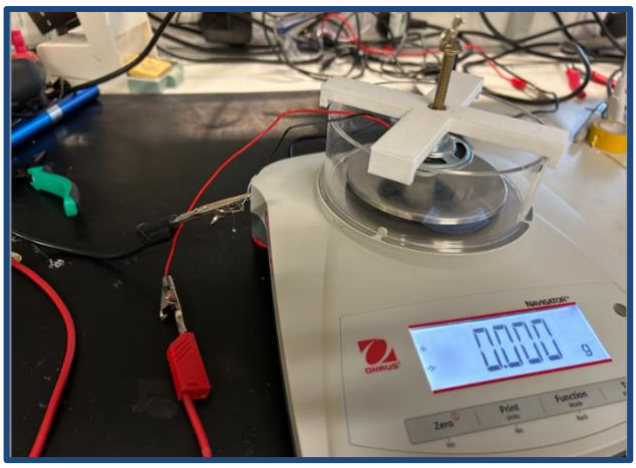

Figure 6: Voice coil testing setup.

The selected stepper motor offers 2048 steps per revolution, which when coupled with an M6 bolt of 1mm pitch (Appendix P: Data Sheets), achieves a linear displacement resolution of 0.488µm (Appendix I). However, imperfections on the screw thread, friction in the nut and errors in the stepper motor may impact this precision – issues that can be mitigated by using high-quality components and lubricant.

The stepper motor is controlled by an Arduino Nano microcontroller (Appendix P: Data Sheets), with the programming logic detailed in the pseudocode (Appendix N) and outlined in Figure 7. Users have flexibility to specify either a target force or deformation. The UI (Appendix M) transmits commands to the Arduino via the serial port, which then sets parameters such as target force, target deformation and the compression rate. This configuration ensures precise control over the testing process, allowing for adjustments based on input from the UI.

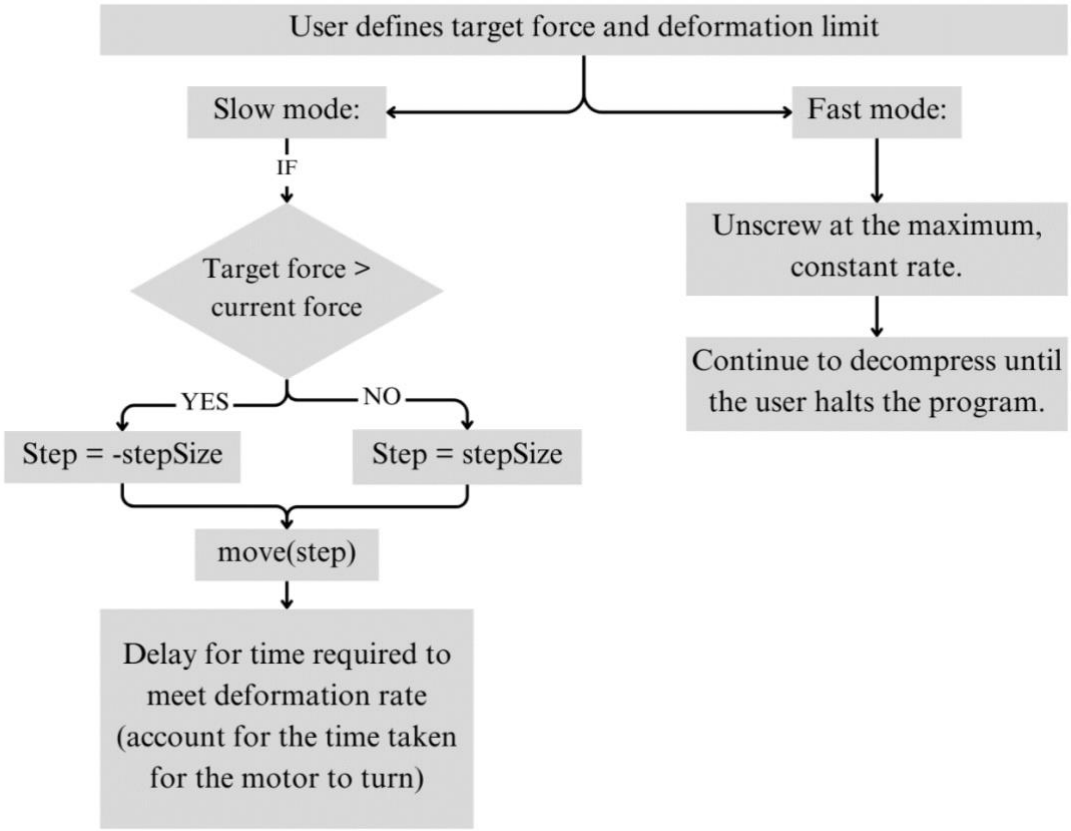

Figure 7: Flow chart outlining the process of the Arduino program for compression and decompression control of the motor. Steps must be an integer, the error is fed back into the main function and accounted for in the next step. For example: Number of steps = 2.5, the motor moves 2 steps and the 0.5 step error is accounted for on the next loop.

3.6 Force Sensing

The project considered options from the Decision Matrix, ultimately focusing on two: a load cell for its precision and a spring for its cost-effectiveness. The load cell design incorporated a proportional (P) feedback loop (Figure 8), as identified from the . This feedback system used a P term to align the applied force with the desired force and was implemented via the Arduino. This setup enabled the precise application of desired forces by adjusting the stepper motor's displacement accordingly.

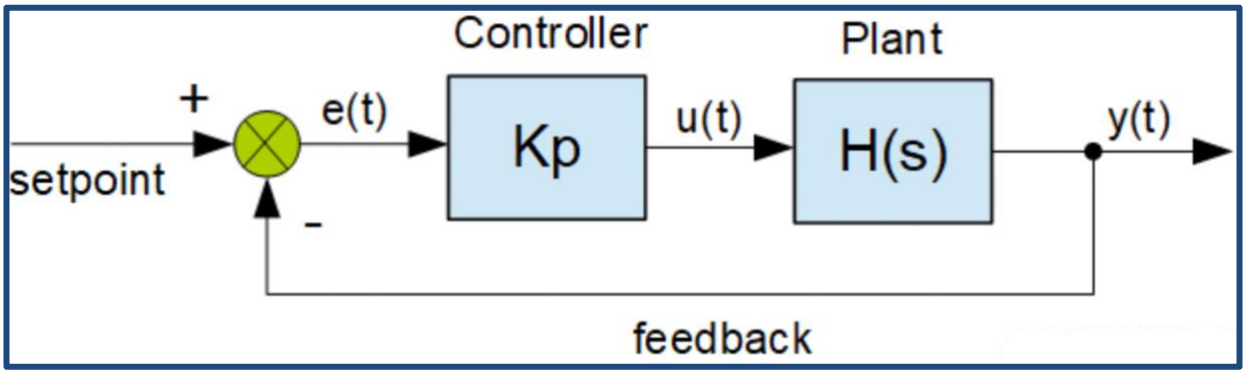

Figure 8: Diagram of operation of Proportional (P) controller with e(t) representing the error signal, u(t) representing the system input, y(t) representing the output signal, Kp representing the proportional gain and H(s) being the system function [16].

For the calibrated spring prototype, the spring constant was first determined experimentally. To calibrate the spring, a known force was applied using the load cell equipped device and the resulting displacement was measured. A force-displacement graph was generated from these measurements (Figure 9) and the spring constant was calculated from the gradient of this linear relationship. During operation, based on the spring constant, an Arduino program translates the displacement of the screw into a force output – allowing the spring to function similarly to the load cell.

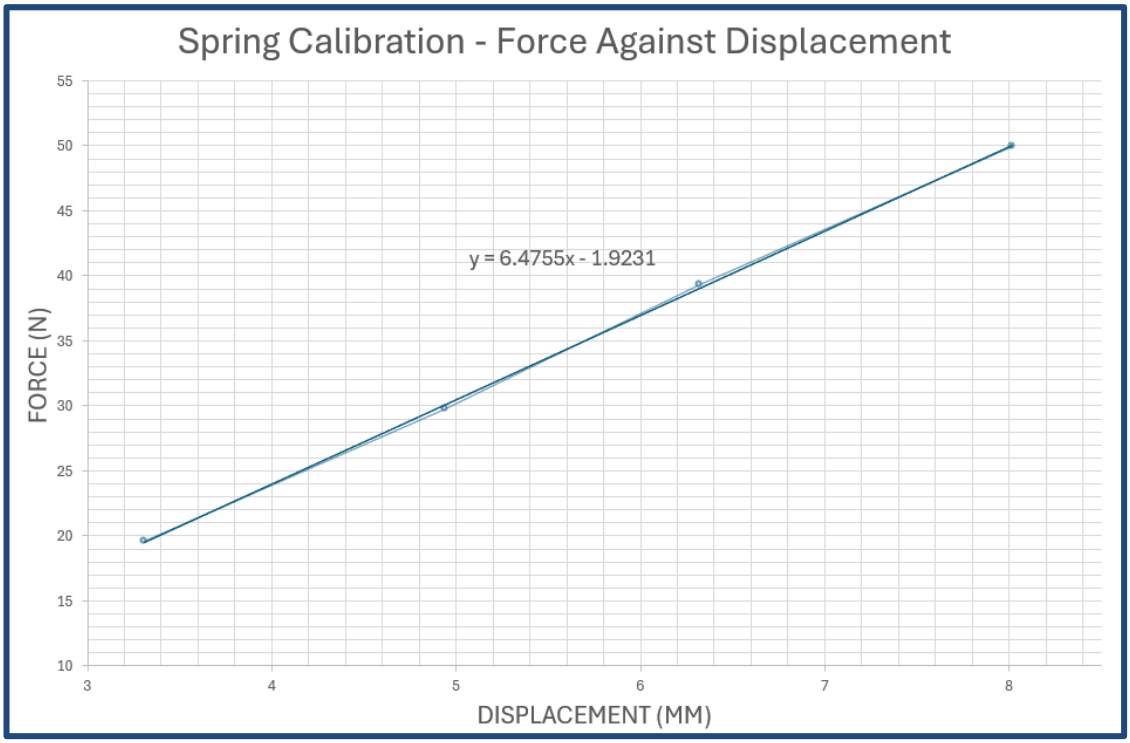

Figure 9: Graph of force against displacement for the spring under compression. The gradient was calculated to find the spring constant.

3.7 Imaging

Evaluating various imaging techniques, including ultrasound and light microscopy, OCT was chosen for its rapid acquisition speeds, important for capturing the processes of compression and decompression in real-time (Appendix P). Additionally, its high penetration depth allows visualisation of deformation across the entire thickness of the sample, providing insights into how mechanical forces affect internal structures. Figure 10 outlines the mechanism of OCT. [17]

Early trials of the 3D acquisition function with both plant and sponge samples displayed issues with backscattering, meaning sufficient depth detail could not be captured. Furthermore, an insufficient number of unique data points hindered the effectiveness of subsequent image processing. After consultation with OCT device's manufacturer (Thorlabs), it was determined that OCT was not suitable for the project's objectives.

Consequently, the magnified video feed of the OCT device was used to capture 2D top-down images of the sample during the compressive loading and unloading phases. Although a USB light microscope may have offered better clarity and superior surface detail, its use was limited by accessibility. This approach allowed the project to continue with minimal compromise.

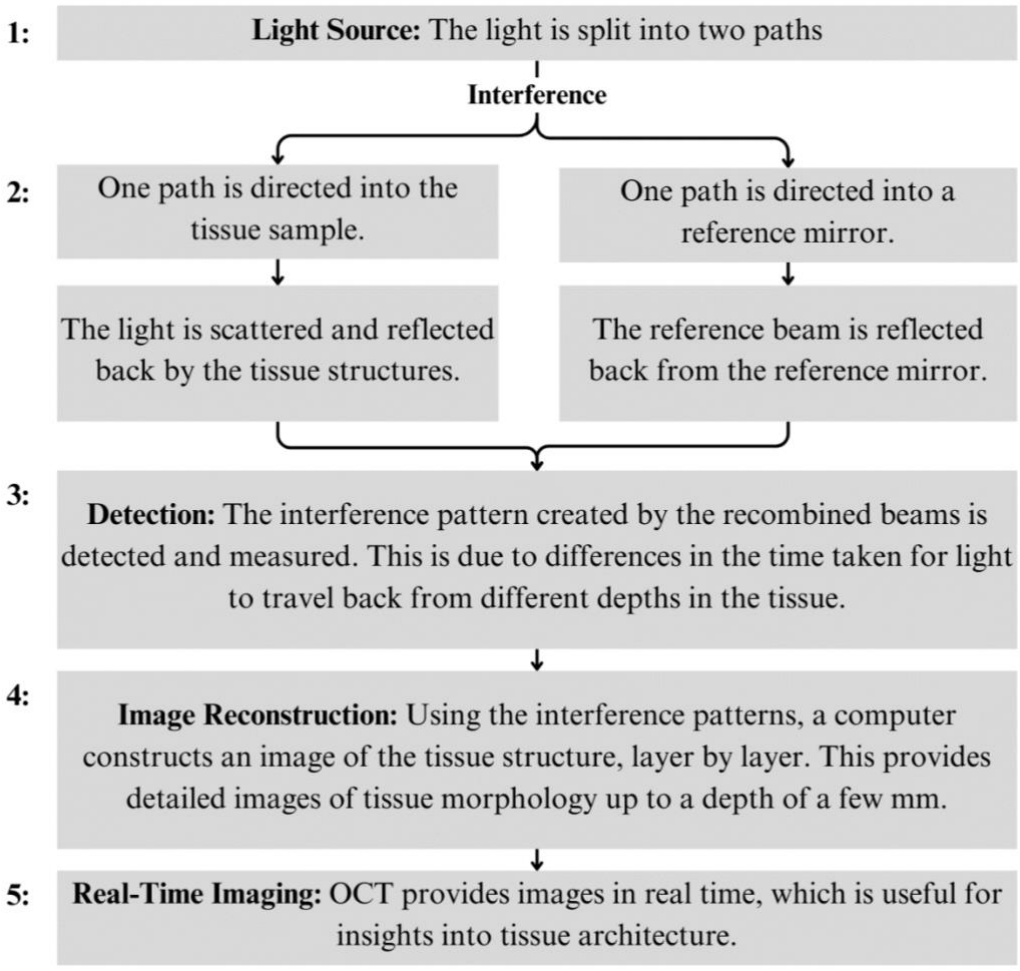

Figure 10: Flow diagram of OCT operation.

3.8 Image Processing

Each image undergoes greyscale conversion before being added to a 4D array, representing x-direction, y-direction, pixel intensity and frame number. Pores are isolated on each frame by the process outlined in Figure 11. Pores are tracked across frames by identifying the pore in the subsequent frame that is closest to the pore in the current frame, as determined by the smallest Euclidean distance between pore centroids. However, limitations arise from low frame rates or pore isolation inaccuracies. Adequate frame rates are essential to maintain pore tracking accuracy and ensure that movements of pores are limited between any two frames. A list of pore locations is generated per frame and successful tracking is manually verified. Displacement is determined between the first and last frames and a map is created using linear interpolation between tracked pore points [18].

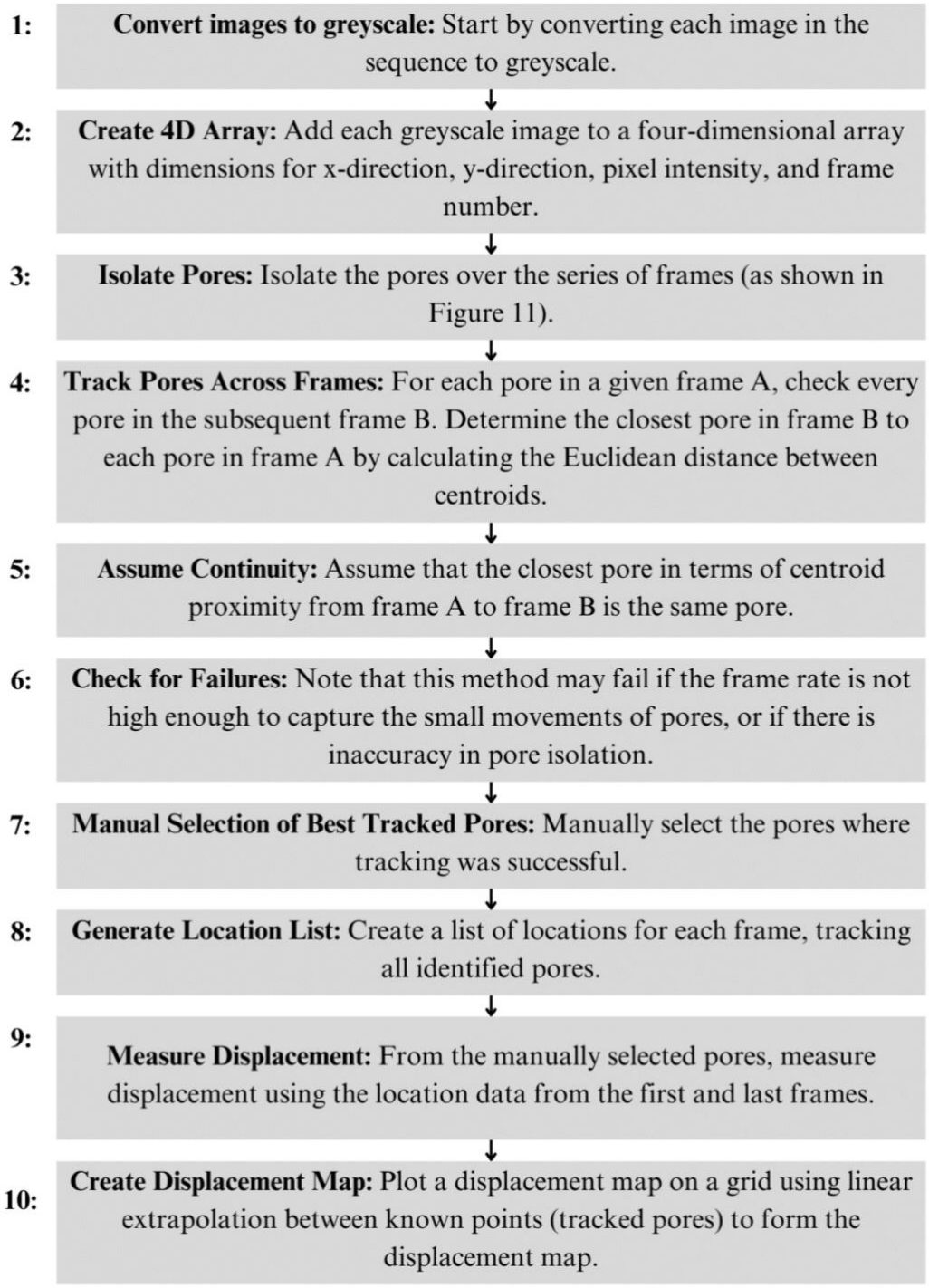

Figure 11: Flow diagram of pore isolation process for displacement map generation.

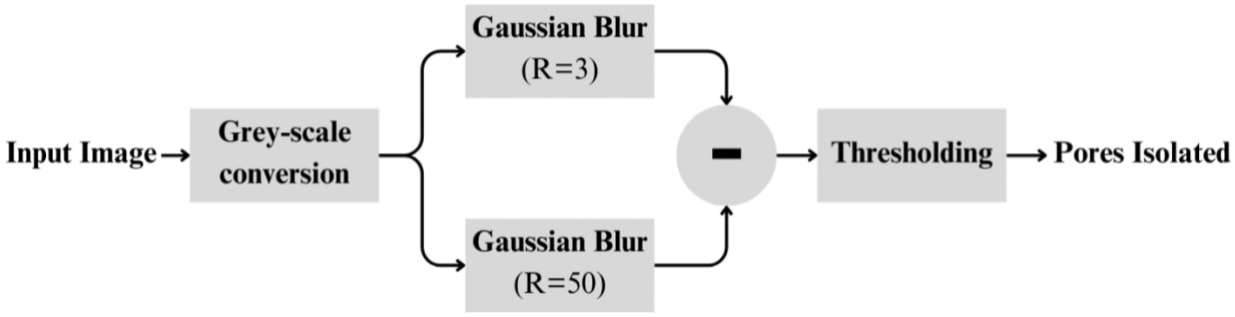

Figure 12: Flow diagram of pore isolation procedure. Blur radii were chosen based on best performance at isolating pores.

3.9 Testing Plan

Testing was focused on the load cell prototype due to buckling observed in preliminary testing of the calibrated spring prototype (Appendix K) and time constraints. This ensured a more efficient use of available resources, allowing deeper analysis of the load cell prototype. Figure 13 shows the testing setup.

3.9.1 Global Mechanical Properties

Three sponge samples were cut from the same block and tested using the device to gather data for stress-strain relationships and to calculate the elastic moduli. One sponge was tested in both its wet and dry states. For uniformity, wet sponges were hydrated with 0.1mL of distilled water using a pipette prior to each experiment. Three repeated experiments were conducted on each sponge sample to increase reliability. The testing procedure consists of a 6-minute 40-second compression phase at a 0.005mm/s compression rate, followed by a 7.5-minute hold phase and a 1-minute decompression phase. The OCT time-series function was set up at 20, 30 and 2 second intervals during compression, holding and decompression respectively.

3.9.2 Pore Analysis

As detailed in Section 3.8, image processing code used image frames in tandem with force data recorded by the device to track the deformation of individual pores

3.9.3 Displacement Map

A displacement map was generated to illustrate the local mechanical variations within the sample during compression, highlighting its potential for application with biological tissues.

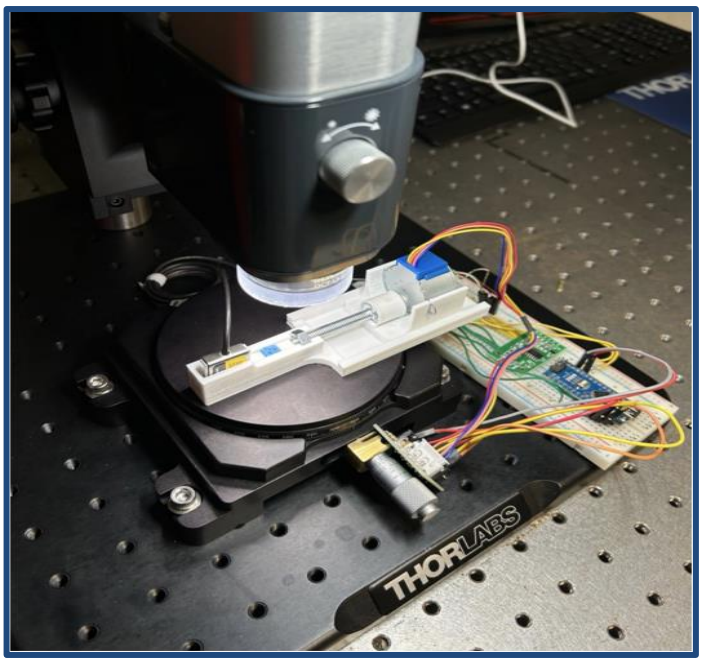

Figure 13: Image of testing setup under the OCT device.

3.10 Ethics & Risk Assessment

Given that the project only used small quantities of non-GM plant tissue and did not involve mammalian tissue, no significant ethical concerns were raised and ethical approval was not required.

Project decisions were guided by a DFMEA (Appendix F), which provided insights into potential failure points of the device and strategies for risk mitigation. Additionally, a risk assessment (Appendix D) was conducted to ensure safety during device operation.

4 Results

4.1 Global Mechanical Properties

Figure 14, 15 and 16 are plots made from data recorded by the device. A Shapiro-Wilk test ($p \approx 0$), for normality and a Kruskal-Wallis test ($p=0.09$) for significant difference in the medians was performed on the wet sponge data in Table 4.

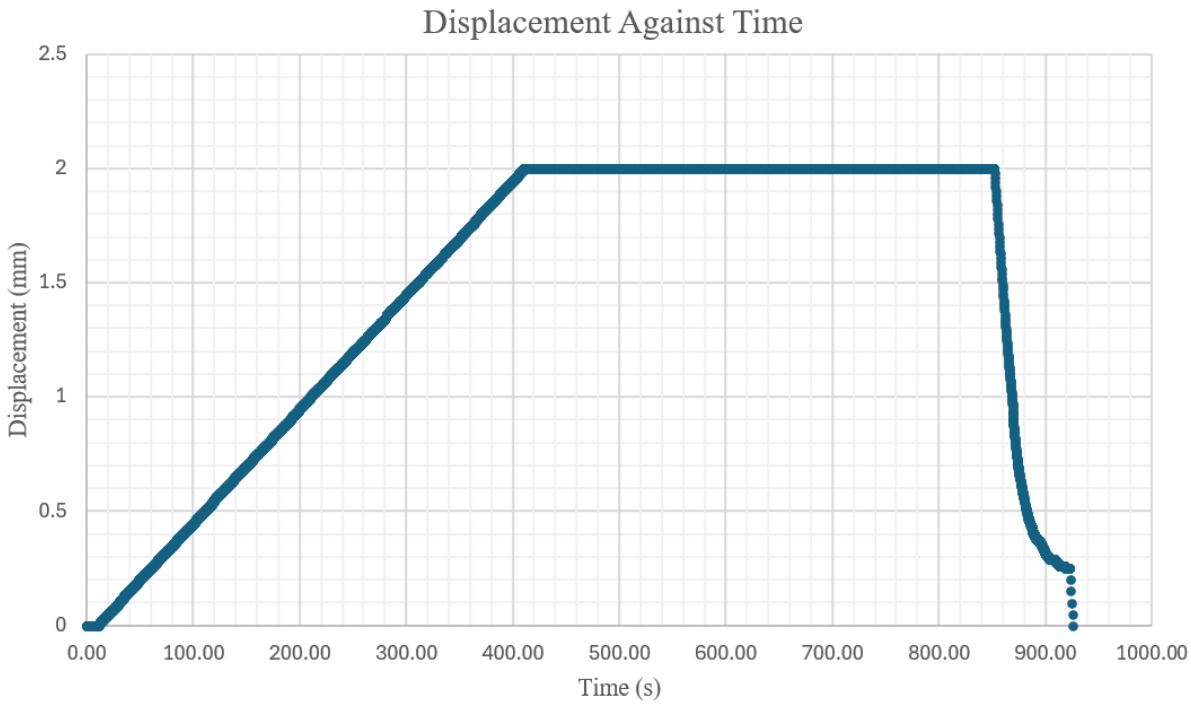

Figure 14: Displacement-time graph for sponge 1, test 1. The compressive phase runs from 0-400s, hold phase runs from 400-850s and the decompression phase runs from 850-910s. Linear compression was applied, with non-linear decompression which slows as it approaches zero force.

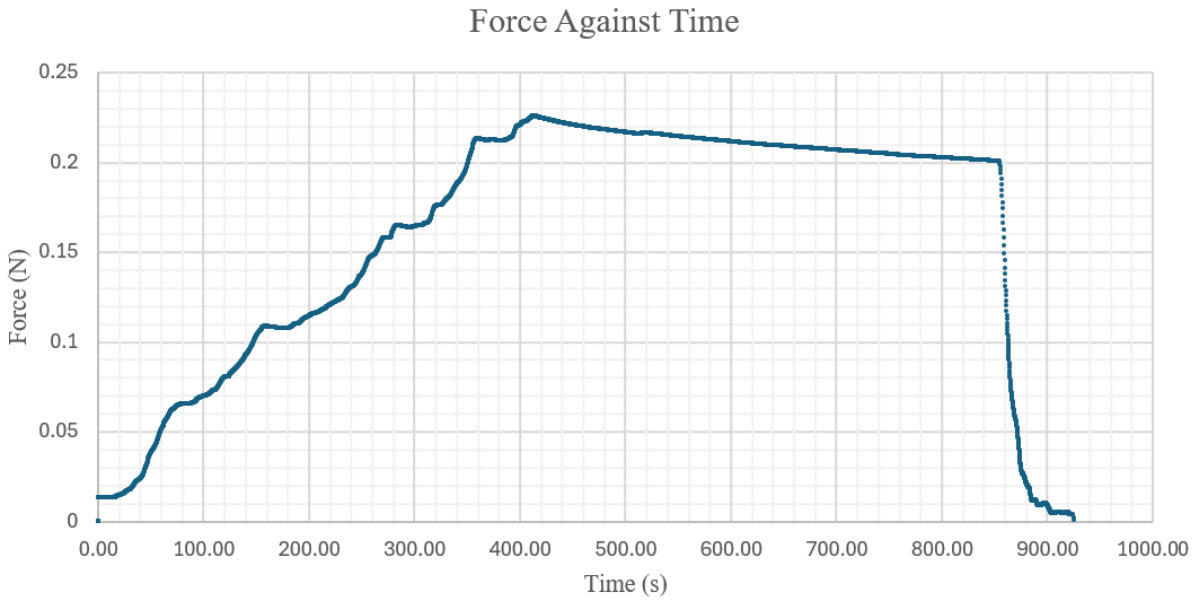

Figure 15: Force-time graph for sponge 1, test 1. Force increases approximately linearly with some deviation and a stress relaxation effect can be observed during the hold phase. Again, decompression was non-linear.

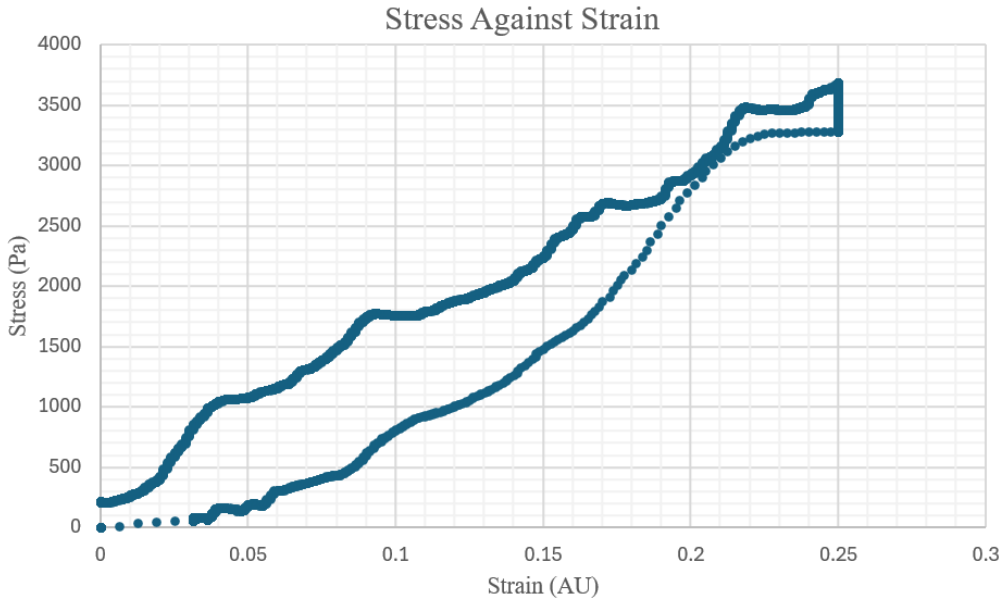

Figure 16: Graph of stress against strain for sponge 1, test 1. A hysteresis effect is observed in the differences between the compressive and decompressive curves. The area under the hysteresis was calculated in MATLAB as 163.65N/m^2. Accounting for sample volume the energy loss was calculated as 0.0802mJ.

Table 4: Elastic moduli of sponge samples. Sponges 1 and 2 were tested in a wet state with sponge 3 tested in both a wet and dry state. All samples were compressed under the same thresholds of either a 25% deformation or a force of up to 80g. This force was only reached by the dry sponge as the deformation limit was reached first by the wet sponges at a force of ~20g (as shown in Figure 15). A Kruskal-Wallis found no significant differences between the median elastic moduli of the wet sponges (p=0.09)

Sponge	**Test**	**Elastic Modulus (kPa)**	**Sponge Type**	**Mean Elastic Modulus (kPa)**
1	1	13.8	Wet	11.8
	2	11.7		
	3	10.0		
2	1	12.1	Wet	12.8
	2	16.1		
	3	10.3		
3	1	10.2	Wet	9.82
	2	9.79		
	3	9.81		
	1	931	Dry	780
	2	587		
	3	823		

4.2 Pore Analysis

As outlined in 3.8, analysis was performed on one pore of sponge 2, test 1. A pore was isolated and its height and width were tracked (Figure 19).

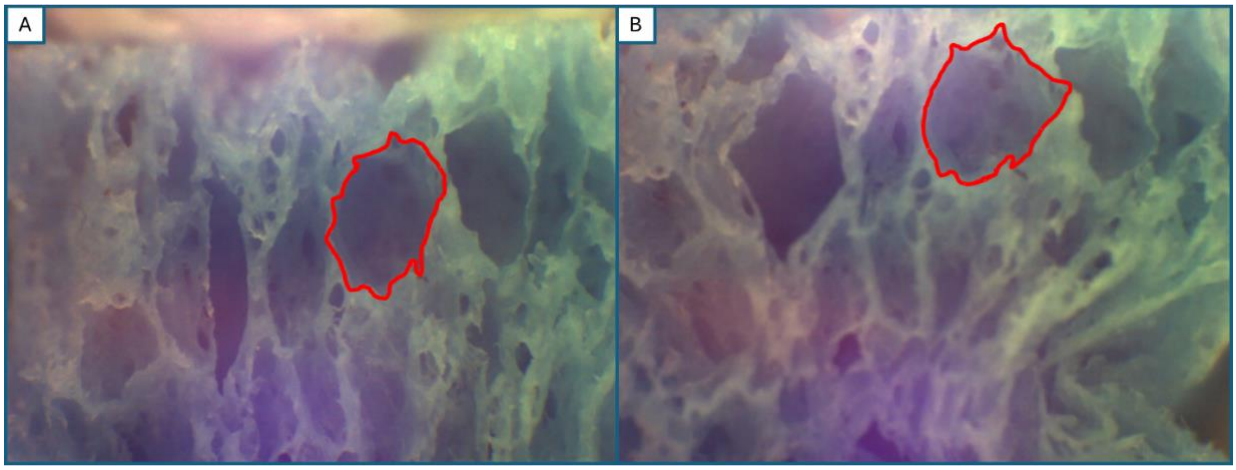

Figure 17: OCT video feed image of sponge 2, test 1. The red outline shows the chosen pore for analysis. (A) Initial uncompressed state (B) Peak compressed state. During compression the sponge displays some buckling at the bottom right corner of the image inwards, towards the left.

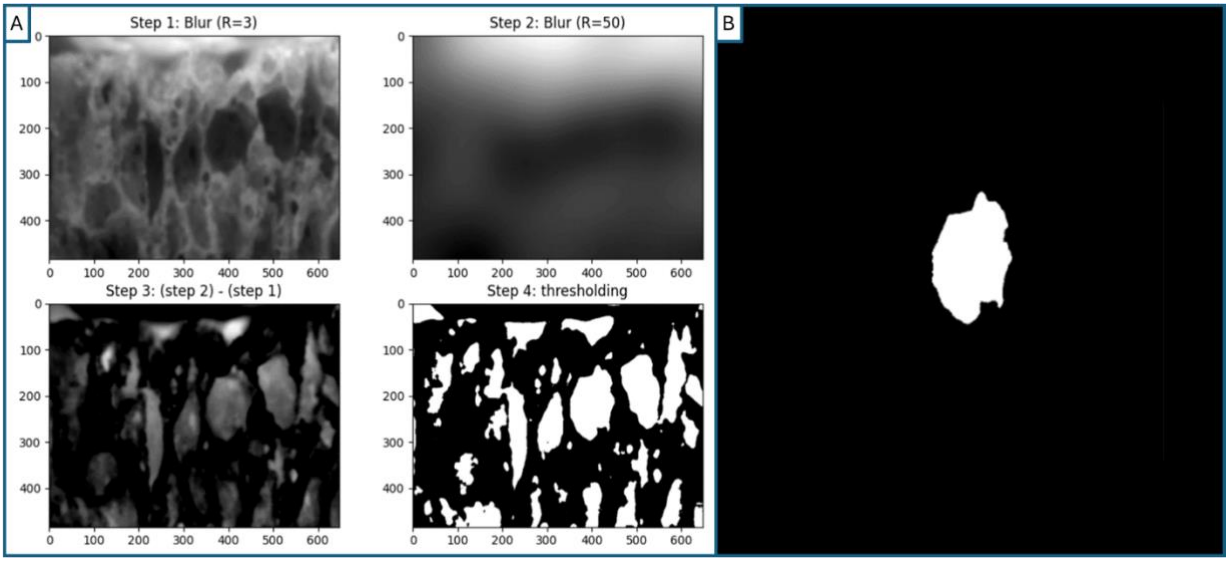

Figure 18: Steps of image processing. (A) Steps 1-4 show the output of each step in the process outlined in section 3.8. (B) Isolated pore.

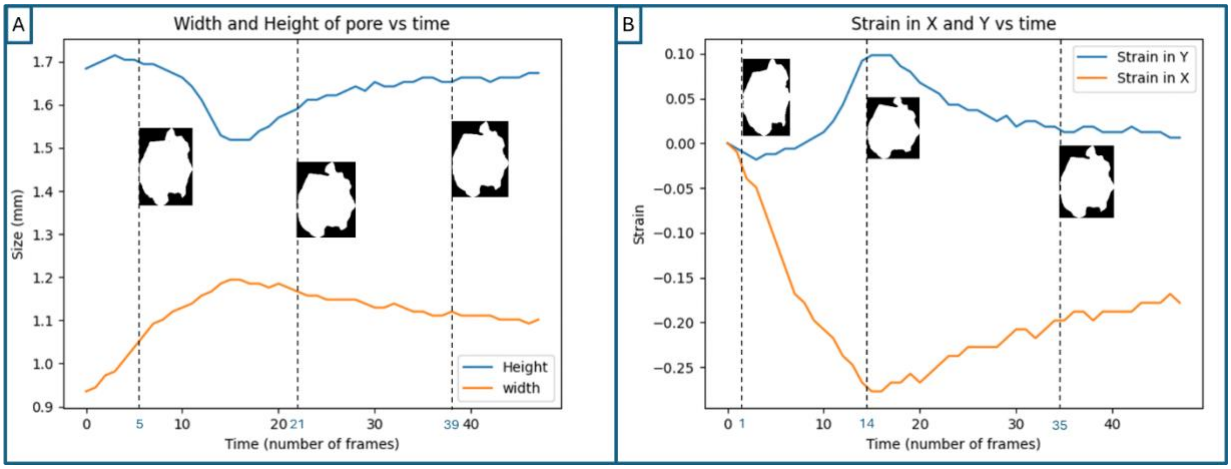

Figure 19: Plots showing changes in the chosen pore's size over time. Peak compression occurs at frame 15. (A) Width and height of the pore against time. Corresponding pore isolation images are shown at frames 5, 21 and 39. (B) Strain in x and y directions against time, where compressive strain is defined as positive. Corresponding pore isolation images are shown at frames 1,14 and 35.

4.3 Deformation Map

As outlined in 3.8, a plot of displacement vectors (Figure 21) and a displacement map (Figure 22) were produced.

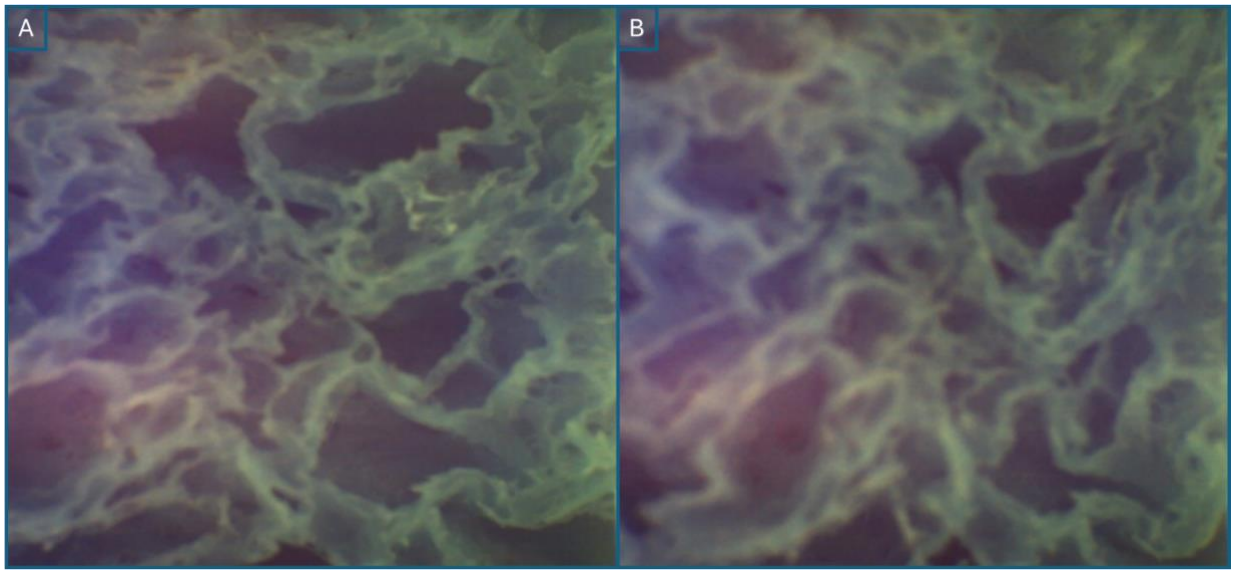

Figure 20: OCT video feed images of sponge 1, test 1: (A) Initial uncompressed state. (B) Peak compressed state.

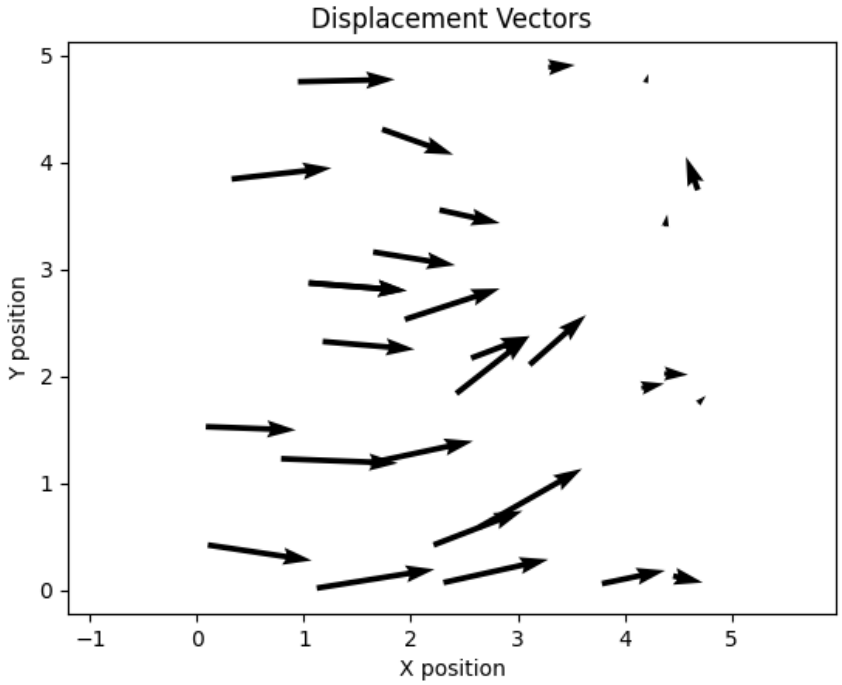

Figure 21: Displacement vectors showing the trajectory of each tracked pore from its initial uncompressed state to its peak compression state.

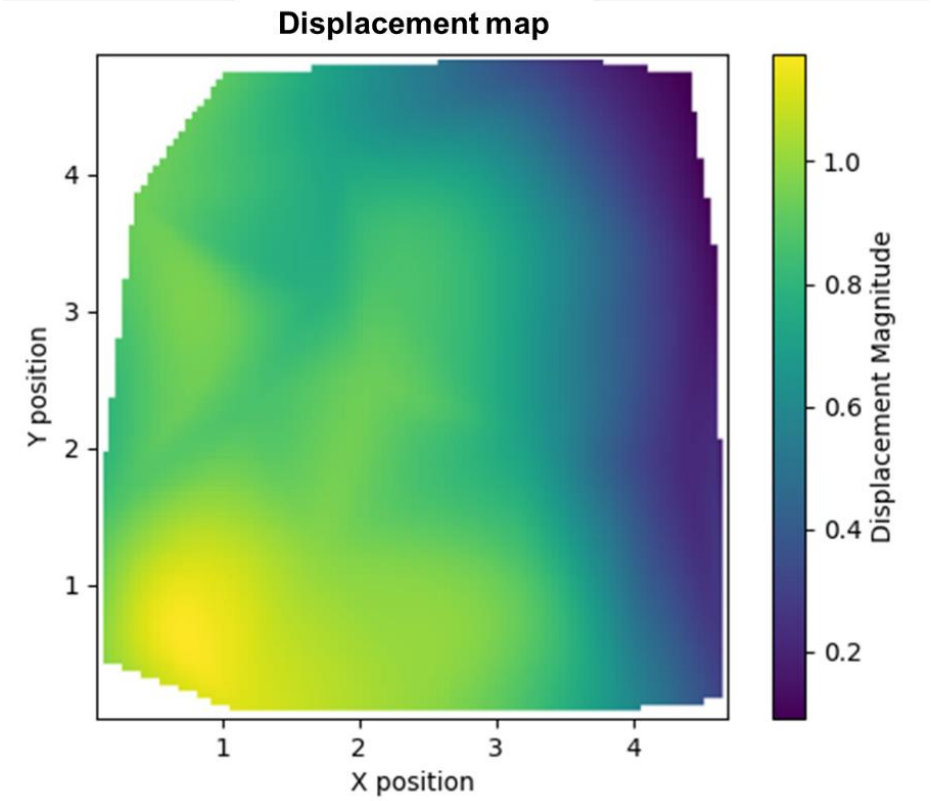

Figure 22: Displacement map of the sample shown in Figure 20. Local variations in displacement are shown as a heat map developed from linearly interpolating between the magnitude of the vectors shown in Figure 21. The sample was compressed from left to right with the block on the side of the load cell acting as a fixed wall (right). Pixels closer to yellow indicate more local displacement than pixels closer to purple. Reduced displacement is observed on the right.

5 Discussion

5.1 Interpretation of Results

5.1.1 Global Mechanical Properties

A Shapiro-Wilk test confirmed non-parametric distribution of the elastic moduli ($p \approx 0$), leading to the choice of a Kruskal-Wallis test which found no significant differences between the median elastic moduli of the wet sponges ($p=0.09$). This consistency across multiple measurements may support the repeatability and reliability of the testing device. It is important to acknowledge that the uniformity of the wet sponge samples' elastic moduli may be uncertain due to water content and pore size variability. Despite this, the fact that all samples originated from the same source supports the assumption of uniform elastic moduli, which is consistent with the observed data. Overall, it is difficult to draw conclusions on the accuracy of the device's ability to characterise global mechanical properties. Future efforts to validate its accuracy should include testing with larger sample sizes and comparison to measurements from a recognised industry-standard device, such as the Instron 6800 [11]. Regrettably, this validation could not be conducted because of limited access to the necessary equipment and time restrictions.

Sponge number 5 exhibited distinct elastic moduli in its wet and dry states, consistent with the principle that reduced water content correlates with an increased elastic modulus [19]. Again, further validation is required to confirm the accuracy of this observation.

The device was operated in deformation application mode and the sample was compressed to 25% of its initial length, held at this deformation and then decompressed. The force-time graph (Figure 15) illustrates a linear increase in force overtime as the stepper motor operated and increased the displacement of the screw, with a few irregularities. It is suspected that these deviations arose from the force application mechanism, due to friction between the compression blocks and the housing floor – further supported by visual observation during testing.

Additionally, a hysteresis effect was observed in the stress-strain graph (Figure 16) which describes the difference in energy between the loading and unloading phases (calculated at 0.0802mJ). It is suspected that this discrepancy between energy input and recovery is due to internal friction within the cellulose sponge's structure leading to thermal energy dissipation. This behaviour underscores the viscoelastic properties of the cellulose sponge, consistent with findings by Tjahjanto et al. for cellulose-based materials [20]. This is further supported by the stress relaxation observed during the holding phase, where the measured force decreases at constant deformation.

5.1.2 Pore Analysis

The individual pore analysis (4.2) highlights the device's capability to track changes in pore size, underscoring the effectiveness of the device in studying anatomical changes. Image processing effectively utilised data from the device, in conjunction with imaging, to create a displacement-time graph (Figure 14). This analysis demonstrates that during compression of the sample, this specific pore underwent compression in the y-axis and tension in the x-axis.

5.1.3 Displacement Map

The displacement map (Figure 22) demonstrates the device's capability to quantify local displacement variations within the sample, yet with limited resolution from only 25 centroids. Linear interpolation between displacement vectors was used, but due to the sparse data, linearity between any two points may be compromised. To enhance the accuracy of future strain mappings, several improvements can be considered: increasing the number of structures tracked, utilising imaging techniques with higher frame rates and refining the point tracking algorithm [21]. Current methods such as digital image correlation rely on speckle patterns to generate numerous unique points for tracking [22]. In contrast, the method outlined in 3.8 is better suited for the project, as it can track the sample's inherent structures without needing external modification.

5.1.4 Sample Selection

As discussed in Section 3.3, the cellulose sponge was chosen for its uniform mechanical properties. Furthermore numerous, large pores facilitated effective image processing during proof-of-concept testing. However, the inability of cellulose sponge to undergo remodelling meant it was unsuitable for evaluating the device's ability to characterise this process. Consequently, the device's performance in terms of sample preservation and sterility could not be thoroughly evaluated and these aspects were not prioritised. To fully test the device against this objective, advancing to experiments with plant tissue is necessary.

5.2 Evaluation of Design

5.2.1 Housing

The housing chamber successfully held samples stationary in the field of view of the microscope - crucial for characterisation. Moving forwards to plant testing, enhancements are required to address the objective of sterility and sample preservation. To sustain and hydrate plant tissues, a 0.3% agar solution is recommended as an imaging compatible, nutritional medium [23, 24]. For the load cell prototype, compartmentalisation is required to protect sensitive components from humidity-related damage. The calibrated spring prototype would be easier to adapt for plant cell testing as it is not impaired by humidity. In contrast to the load cell prototype, the calibrated spring can be sterilised using autoclaving, which uses pressurised steam to eliminate microbial contaminants [25].

Achieving sterility was challenging due to difficulties in preventing parts from moving in and out of the sterile field, which risked introducing contaminants. A proposed solution was to isolate the motor from the bolt and replace the bolt adapter with a magnet array to transmit rotational motion through the wall of a sealed chamber. While efforts were made to achieve this, time constraints and the expensive nature of these parts led to prioritisation of the other key objectives.

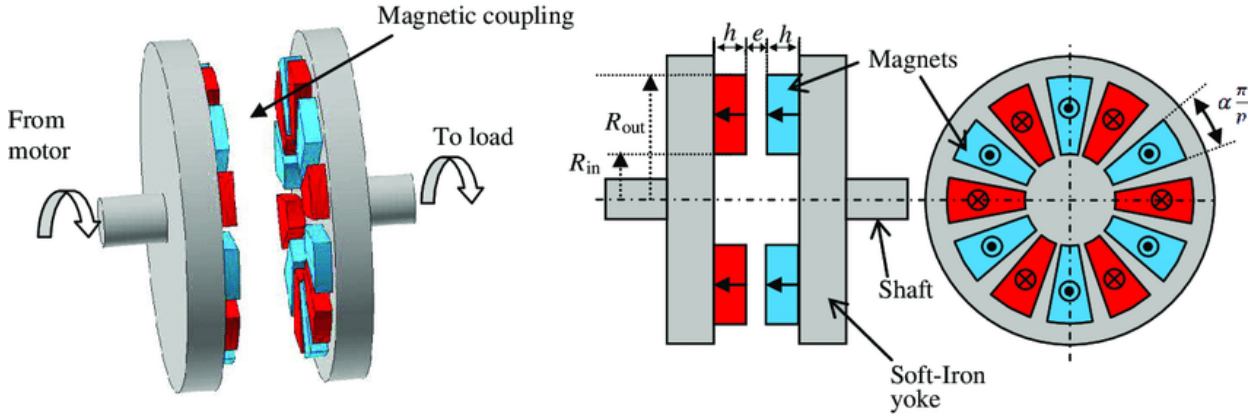

Figure 23: Schematic showing magnetic coupling method for sterile force application [26]

5.2.2 Force Application

The device effectively applied high-resolution, controlled compressive forces to samples over extended periods. The force specification mode offers a high resolution of 1mN (dependent on the load cell resolution due to feedback, Appendix P), while the deformation control mode provides a precision of 0.49µm (Appendix I). Additionally, users can adjust the rate of compression or force application according to their specific research needs. The device's dual-mode functionality and high resolution enhance its versatility and positions it competitively alongside existing devices (2.3).

The usability of the device could be improved by developing a more advanced UI (Appendix M). The updated interface should feature a live force plot and allow scheduled changes in applied force - eliminating the need for continuous manual adjustment. Time constraints prevented assessment of the device's ability to maintain applied force over a 14-day period which is an important feature for characterising remodelling when

progressing to plant testing. However, the device successfully applied a constant force for three days without overheating or encountering any issues that may suggest limitations in extended force application. For future tests, one potential improvement could involve using a more effective lubricant to decrease friction on the blocks - increasing the uniformity and accuracy of force application.

5.2.3 Force Sensing

The load cell prototype was successful in sensing the applied force and providing feedback, allowing high resolution and accurate force measurement. P control was selected for the target force mode due to its precise force application and minimal steady state error. Further research identified issues with integral (I) wind-up and volatility of the derivative (D) controller [27, 28], leading to the decision that full PID control was unnecessary given the prototype's effective performance.

Integrating feedback into the calibrated spring prototype proved to be challenging due to the difficulty in measuring force instantaneously, increasing the risk of overshooting the desired force and damaging the sample. Moreover, the spring was prone to buckling during testing (Appendix K), which reduced the accuracy of its force measurement. This issue could potentially be addressed by replacing the current spring with a conical spring [29]. Furthermore, integrating feedback into the calibrated spring prototype could be achieved by incorporating proximity sensors, such as Hall Effect sensors, to monitor compression in real-time. [30].

5.2.4 Imaging

OCT was initially chosen for its accessibility in the lab, depth imaging capabilities and rapid imaging capabilities [17]. However, challenges were encountered during early trials with plant stem tissue, particularly due to resolution issues with the 3D image acquisition function. The low-resolution images obtained (Appendix J) provided insufficient detail for effective image processing and thus mechanical characterisation of local properties. Additionally, significant backscattering occurred when testing with sponge samples due to light trapping in the pores, a prominent problem with OCT [31]. Consequently, the device's video camera was used instead for its ability to capture unique points for image processing and provide a comprehensive view for whole sample analysis, crucial for displacement map generation. Ultimately, the scanning function of the OCT proved unsuitable for the current device setup, suggesting that an alternative imaging modality would be necessary for 3D data acquisition using plant samples in future testing. If OCT were to be used again, improved axial resolution could be obtained by employing a deep-learning algorithm which spatially resamples the obtained images [32].

5.2.5 Whole Device Functionality & Future Directions

For evaluation, a key objective analysis was conducted for each prototype (Appendix H).

In proof-of-concept testing with sponge, the load cell prototype achieved all key objectives except sterility and sample preservation. It offers high resolution control over user-specified compressive force and deformation, advantageous over many existing devices which are restricted to tensile force application [9]. Users can control the deformation or force application rate and sustain a constant compression. It effectively records global mechanical properties and allows characterisation of local mechanical properties and anatomical changes. As detailed in the expense sheet (Appendix G), both prototypes met the device's affordability criterion, with the calibrated spring prototype proving more cost-effective at £19 compared to the £740 load cell prototype. Despite its higher cost, the load cell prototype remains an affordable option for further prototyping as it is substantially cheaper than commercial alternatives such as the Linkam Modular Force Stage (£48,000). For plant tissue testing, additional compartmentalisation within the housing chamber is necessary to enable sample immersion in nutrient media and sterilisation through implementing a hermetic seal. Improvements such as constructing the housing from metal and using lubrication can minimise inaccuracies in force application caused by friction (5.2.2).

The calibrated spring prototype, while cost-effective, faced challenges such as spring buckling and lacked a direct feedback system into the force applicator. Due to time constraints and the buckling issue its testing was prevented and time was devoted to load cell prototype. For future iterations, incorporating position sensors could monitor and provide feedback, however integrating these sensors would bring additional challenges,

particularly in sterilising the electrical components through autoclaving. Addressing the buckling problem may involve switching to a conical spring design or using an alternative elastic material with known mechanical properties, such as silicone, to improve accuracy of force application [33].

However, before advancing to biological tissue testing, further testing and validation is essential through using a diverse range of samples and comparison to measurements of an industry-standard device. Moreover, a broader range of non-invasive imaging techniques, such as ultrasound, should be explored in conjunction with our device to accurately identify variations in tissue architecture with loading.

6 Conclusion

In conclusion, the developed prototypes address the limitations of high cost and resource-intensive existing devices. They present a promising avenue for an affordable and accessible means to study tissue mechanics, with the potential to assist research in fields such as stress priming, GM crops and disease diagnostics. The device effectively applies precise compressive loads to a cellulose sponge sample and allows characterisation of global and local mechanical properties. However, further testing and validation are required to ensure its accuracy. Future iterations will seek to incorporate sterility and refine the spring prototype to match load cell functionality without sacrificing affordability, with the next phase of testing being extended to biological tissue samples. Ultimately, the project offers a stepping stone for future advancements in studying tissue mechanics and understanding the tissue remodelling processes.

7 References

1. Frost HM. Wolff's Law and bone's structural adaptations to mechanical usage: an overview for clinicians. The Angle Orthodontist [Internet]. 1994 ;64(3):175–88. Available from: https://pubmed.ncbi.nlm.nih.gov/8060014/
2. Brenya E, Pervin M, Chen Z, Tissue DT, Johnson S, Braam J, et al. Mechanical stress acclimation in plants: Linking hormones and somatic memory to thigmomorphogenesis. Plant, Cell & Environment. 2022 Jan 18;45(4):989–1010. https://doi.org/10.1111/pce.14252.
3. Kouhen M, Dimitrova A, Scippa GS, Trupiano D. The Course of Mechanical Stress: Types, Perception, and Plant Response. Biology [Internet]. 2023 Feb 1 ;12(2):217. https://doi.org/10.3390/biology12020217.
4. Chaffey N, Cholewa E, Regan S, Sundberg B. Secondary xylem development in Arabidopsis: a model for wood formation. Physiologia Plantarum. 2002 Apr;114(4):594–600. https://doi.org/10.1034/j.1399-3054.2002.1140413.x.
5. Kendall SL, Holmes H, White CA, Clarke SM, Berry PM. Quantifying lodging-induced yield losses in oilseed rape. Field Crops Research. 2017 Sep;211:106–13. https://doi.org/10.1016/j.fcr.2017.06.013.
6. Iida H. Mugifumi, a beneficial farm work of adding mechanical stress by treading to wheat and barley seedlings. Frontiers in Plant Science [Internet]. 2014 Sep 12;5. https://doi.org/10.3389/fpls.2014.00453.
7. Ansardamavandi A, Tafazzoli-Shadpour M, Omidvar R, Jahanzad I. Quantification of effects of cancer on elastic properties of breast tissue by Atomic Force Microscopy. Journal of the Mechanical Behavior of Biomedical Materials. 2016 Jul;60:234–42. https://doi.org/10.1016/j.jmbbm.2015.12.028.
8. Velasco MA, Narváez-Tovar CA, Garzón-Alvarado DA. Design, Materials, and Mechanobiology of Biodegradable Scaffolds for Bone Tissue Engineering. BioMed Research International [Internet]. 2015;2015:1–21. https://doi.org/10.1155/2015/729076.
9. Robinson S, Huflejt M, Barbier de Reuille P, Braybrook SA, Schorderet M, Reinhardt D, et al. An Automated Confocal Micro-Extensometer Enables in Vivo Quantification of Mechanical Properties with Cellular Resolution. *The Plant Cell*. 2017;29(12): 2959–2973. https://doi.org/10.1105/tpc.17.00753.
10. ADMET BioTense. System Brochure BioTense Bioreactor [Internet]. Available from: https://www.admet.com/wp-content/uploads/2015/07/ADMET-BioTense-Bioreactor-System-Brochure.pdf
11. Linkam. MFS Brochure [Internet]. Linkam Scientific. Available from: https://www.linkam.co.uk/mfs-brochure
12. 6800 Series Universal Testing Systems [Internet]. Available from: https://www.instron.com/en/products/testing-systems/universal-testing-systems/low-force-universal-testing-systems/-/media/literature-library/products/2020/01/6800-series-universal-testing-systems.pdf?la=en&hash=D6DDD212DDD72F6E0ED6A0D5DC910264&_gl=1
13. Plavcová L, Gallenmüller F, Morris H, Khatamirad M, Jansen S, Speck T. Mechanical properties and structure–function trade-offs in secondary xylem of young roots and stems. Journal of Experimental Botany. 2019 Jul 1;70(14):3679–91. https://doi.org/10.1093/jxb/erz286
14. Maleki SS, Mohammadi K, Ji K. Characterization of Cellulose Synthesis in Plant Cells. *The Scientific World Journal*. 2016;2016: 1–8. https://doi.org/10.1155/2016/8641373.
15. McCormmach R. H. A. Lorentz and the Electromagnetic View of Nature. *Isis*. 1970;61(4): 459–497. https://doi.org/10.1086/350681.
16. x-engineer.org. *Proportional (P) controller – x-engineer.org*. x-engineer. https://x-engineer.org/proportional-controller/
17. Kennedy BF, Wijesinghe P, Sampson DD. The emergence of optical elastography in biomedicine. *Nature Photonics*. 2017;11(4): 215–221. https://doi.org/10.1038/nphoton.2017.6.

18. Wilk MP, Urru A, Tedesco S, O'Flynn B. Sub-pixel point detection algorithm for point tracking with low-power wearable camera systems: A simplified linear interpolation. *ResearchGate*. 2017; https://doi.org/10.1109/issc.2017.7983629.
19. Cheng L, Deshpande V, Fleck N. Effect of water content on the constitutive response of a cellulose foam. *European journal of mechanics. A, Solids/European journal of mechanics, A, Solids*. 2023;100: 104992–104992. https://doi.org/10.1016/j.euromechsol.2023.104992.
20. Tjahjanto DD, O. Girlanda, Östlund S. Anisotropic viscoelastic–viscoplastic continuum model for high-density cellulose-based materials. *Journal of the Mechanics and Physics of Solids*. 2015;84: 1–20. https://doi.org/10.1016/j.jmps.2015.07.002.
21. Tomasi C, Kanade T. *Shape and Motion from Image Streams: a Factorization Method|Part 3 Detection and Tracking of Point Features*. 1991 [Accessed 15th April 2024]. https://www.ri.cmu.edu/pub_files/pub2/tomasi_c_1991_1/tomasi_c_1991_1.pdf
22. Dong YL, Pan B. A Review of Speckle Pattern Fabrication and Assessment for Digital Image Correlation. *Experimental Mechanics*. 2017;57(8): 1161–1181. https://doi.org/10.1007/s11340-017-0283-1.
23. Bhatia S. Plant Tissue Culture. *Modern Applications of Plant Biotechnology in Pharmaceutical Sciences*. 2015;(978-0-12-802221-4): 31–107. https://doi.org/10.1016/b978-0-12-802221-4.00002-9.
24. Crespel L, Meynet J. *Murashige and Skoog Medium - an overview | ScienceDirect Topics*. Sciencedirect.com. https://www.sciencedirect.com/topics/agricultural-and-biological-sciences/murashige-and-skoog-medium
25. Prins M, Paulsson M. Sterilisation Methods. *Practical Pharmaceutics*. 2015; 677–693. https://doi.org/10.1007/978-3-319-15814-3_30.
26. *Magnetic Coupling*. Stanford Magnets. https://www.stanfordmagnets.com/magnetic-coupling.html [Accessed 15th April 2024].
27. Peterson D. *Intergral Windup Method in PID Control - Technical Articles*. control.com. https://control.com/technical-articles/intergral-windup-method-in-pid-control/
28. Rajinikanth V, Latha K. I-PD Controller Tuning for Unstable System Using Bacterial Foraging Algorithm: A Study Based on Various Error Criterion. *Applied Computational Intelligence and Soft Computing*. 2012;2012: e329389. https://doi.org/10.1155/2012/329389
29. Patil RV, Reddy PR, Laxminarayana P. Comparison of Cylindrical and Conical Helical Springs for their Buckling Load and Deflection. *International Journal of Advanced Science and Technology*. 2014;73: 33–50. https://doi.org/10.14257/ijast.2014.73.03.
30. Ramsden E. *Hall-Effect Sensors: Theory and Application*. Google Books. Elsevier; 2011. https://books.google.co.uk/books?hl=en&lr=&id=R8VAjMitH1QC&oi=fnd&pg=PP1&dq=hall+effect+sensors+proximity&ots=XzJLGeBz9y&sig=0PHKJAgzh2kk6t5RjlXJ3uWgBR4&redir_esc=y#v=onepage&q=hall%20effect%20sensors%20proximity&f=false [Accessed 15th April 2024].
31. Untracht GR, Chen M, Wijesinghe P, Mas J, Yura HT, Marti D, et al. Spatially offset optical coherence tomography: Leveraging multiple scattering for high-contrast imaging at depth in turbid media. *Science Advances*. 2023;9(27).https://doi.org/10.1126/sciadv.adh5435.
32. Yuan Z, Yang D, Wang weike, Zhao J, Liang Y. Self super-resolution of optical coherence tomography images based on deep learning. *Optics express*. 2023;31(17): 27566–27566. https://doi.org/10.1364/oe.495530.
33. MatWeb. Overview of Materials for Silicone Rubber [Internet]. www.matweb.com. Available from: https://www.matweb.com/search/DataSheet.aspx?MatGUID=cbe7a469897a47eda563816c86a73520&ckck=1

8 Appendix

8.1 Appendix A: Acknowledgements

We are grateful for the support of our supervisors Naomi Nakayama and Sam Mason for their continued support throughout the project. We thank Paschal Egan for assistance within the electrical labs and the Thorlabs OCT applications engineer Malte with help using the OCT device. We also thank the Imperial College Bioengineering Department for the use of their facilities and the funding of the project. We like to thank Sibi Varghese for providing us with plant stem samples and Miguel Hermida for inducting and allowing access to the imaging lab. Finally, we like to thank the Imperial Hackspace team for help in the manufacture of the product.

8.2 Appendix B: Team management

To streamline our process and meet all deadlines, we divided our six-person team into three pairs, each focusing on a distinct component of the device: electronics, imaging, or mechanics. The project unfolded in three stages: design, manufacturing and testing, coordinated through a dynamic Gantt chart that set and adjusted internal deadlines based on task progression.

Here are our key takeaways for future projects:

Order parts early: While our Gantt chart accounted for potential delays, we experienced some pauses waiting for part deliveries. We learned it's crucial to order parts well in advance, especially before predictable downtimes like exams or holidays, to avoid idle periods and maximize productivity upon return.

Post-break productivity plan: Work slowed down around deadlines and holidays, but a return to productivity often took longer than expected. To mitigate this, a detailed action plan following on from breaks would ensure a swift and effective project resumption, addressing both the need for rest and the ramp-up to full productivity.

Cross-team collaboration and communication: Though our sub-team division allowed us to maximise individual skills, it limited overlap and shared understanding, making solo work during absences more challenging. Increasing inter-team collaboration would mitigate the effect of absences which is crucial for a cohesive project.

Early lab logistics: Progress was occasionally stalled by unavailable labs or equipment and awaiting inductions. Identifying lab requirements early and scheduling inductions and lab time in advance would minimise these bottlenecks, keeping the project on track.

By incorporating these insights, future endeavors can maintain momentum and leverage team capacity more effectively.

8.3 Appendix C: Decision Matrix

8.3.1 Appendix C.1: Table

Design Feature	Methods	Rating (1-10)								Score
			Cost	Reliable	Precision	Ease of Use	Imaging Compatibility	Ease of Feedback	Ease of Implementation	Sterility	
		Multiplier:	2	1	1	1	1	0.5	1	1	
Force Application	Rack and Pinion		8	5	3	8		5	8		42.5
	Hydraulics		5	5	7	3		5	3		30.5
	Linear Actuator [1]		6	8	9	9		8	9		51
	Voice Coils [2]		8	3	10	10		9	7		50.5
	Stepper Motor [3]		7	8	9	9		8	9		53
Tissue Housing Materials [4][5][6]	ABS		8	8		9	5		9	4	51
	PLA		9	8		9	5		9	4	53
	Glass		5	8		4	10		4	10	46
	Steel		4	8		5	5		6	10	42
Force Measurement	**Load Cell [7][8]**		3	8	10	10	9	10	10	8	66
	Piezoresistor [9]		5	7	7	8	9	9	8	8	61.5
	Spring		10	6	5	9	8	5	5	9	64.5
	Foam block		8	4	2	8	4	3	5	10	50.5
	Silicon block [10]		9	3	4	8	5	6	5	10	56
	Capacitive resistor		5	7	7	10	7	10	8	8	62

8.3.2 Appendix C.2 References

[1] Sekhar, S, and D Stemler. “Linear Piston Actuators.” Iceweb, 9 Jan. 2002, iceweb.eit.edu.au/Valve/SevereServiceValves/LinearPistonActuators.pdf. Accessed 10 Apr. 2024.

[2] Z. Batts, J. Kim and K. Yamane, "Design of a hopping mechanism using a voice coil actuator: Linear elastic actuator in parallel (LEAP)," 2016 IEEE International Conference on Robotics and Automation (ICRA), Stockholm, Sweden, 2016, pp. 655-660, doi: 10.1109/ICRA.2016.7487191. keywords: {Actuators;Force;Springs;Legged locomotion;Mathematical model;Magnetic cores},

[3] Athani, V. V. *Stepper Motors : Fundamentals, Applications and Design*. *Google Books*, New Age International, 1997, books.google.co.uk/books?hl=en&lr=&id=0m8NTozFZL8C&oi=fnd&pg=PA1&dq=stepper+motor&ots=MG8XQiwLI3&sig=2yF-zylOFhkKwes5JgX7UWBDYo4#v=onepage&q=stepper%20motor&f=false. Accessed 10 Apr. 2024.

[4] Sirjani, E., Cragg, P.J. and Dymond, M.K. (2019). Glass transition temperatures, melting temperatures, water contact angles and dimensional precision of simple fused deposition model 3D prints and 3D printed channels constructed from a range of commercially available filaments. Chemical Data Collections, 22, p.100244. doi:https://doi.org/10.1016/j.cdc.2019.100244

[5] Velling, A. (2020). What Materials Are Suitable for Laser Cutting? [online] Fractory. Available at: https://fractory.com/what-can-laser-cutters-cut/

[6] Umapathi, U., Chen, H.-T., Mueller, S., Wall, L. and Seufert, A. (2015). LaserStacker: doi:https://doi.org/10.1145/2807442.2807512

[7] Kim, T., Aulla Villacres, M., Shim, J., Kwon, O.-S. and Kim, H.-K. (2023). Development

of a differential load cell negating inertial force. Measurement, [online] 223, p.113789. doi: https://doi.org/10.1016/j.measurement.2023.113789

doi: https://doi.org/10.1016/j.measurement.2023.113789

[8] uk.rs-online.com. (n.d.). Everything You Need To Know About Load Cells | RS. [online] Available at: https://uk.rs-online.com/web/content/discovery/ideas-and-advice/load-cellsguide

[9] Tran, A.V., Zhang, X. and Zhu, B. (2017). The Development of a New Piezoresistive doi: 10.1109/TIE.2017.2784341

[10] Schneider, F, et al. “Mechanical Properties of Silicones for MEMS.” IOPScience, IOP Publishing Ltd, 29 Apr. 2008, iopscience.iop.org/article/10.1088/0960-1317/18/6/065008/meta. Accessed 10 Apr. 2024.

8.4 Appendix D: Risk Assessment

Number	Risk Description	Likelihood (1-10)	Severity (1-10)	Score	Mitigating Action	Likelihood after	Severity after	Score after mitigation	Further action required
1	Work in electronics lab and the risks associated with it	2	5	10	Ensure all team members have completed a lab induction for the electronics lab	1	5	5	Speak to Paschal if there are any further concerns
2	Exposed wires could come into contact with skin and lead to electric shock	3	3	9	Make sure all wires are insulated and contained within the product where possible	1	3	3	Review the design criteria if mitigating action is not able to be completed
3	Working with the laser cutter	2	7	14	Ensure all team members that are using the laser cutter have been inducted to use the machine	1	7	7	Speak to B220 Lab team if there are any issues
4	Spring may buckle and launch towards user at high velocity	3	1	3	A lid has been designed for this prototype to prevent the spring from leaving the housing	1	1	1	If the lid affects functionality, review design criteria
5	OCT lens glass may break	2	2	4	Ensure OCT is handled with care	1	2	2	If any damage is done to the OCT, report it to Miguel (Imaging Lab Lead)
6	Fingers may get trapped in the device while force is being applied	2	1	2	There should be no reason to place fingers in the device while it is applying force	2	1	2	If it becomes necessary to put fingers in the device while force is being applied, ensure

									device is turned off
7	Electronics may overheat and start a fire or cause burns	1	7	7	Ensure, in the rare event of fire, team members are aware of protocol	1	7	7	If at any point risk of overheating increases, review design criteria
8	Small parts may be swallowed by children	1	5	5	Ensure the device is kept away from unsupervised children	1	5	5	N/A

8.5 Appendix E: Technical Drawings

8.5.1 Appendix E.1: Adapter

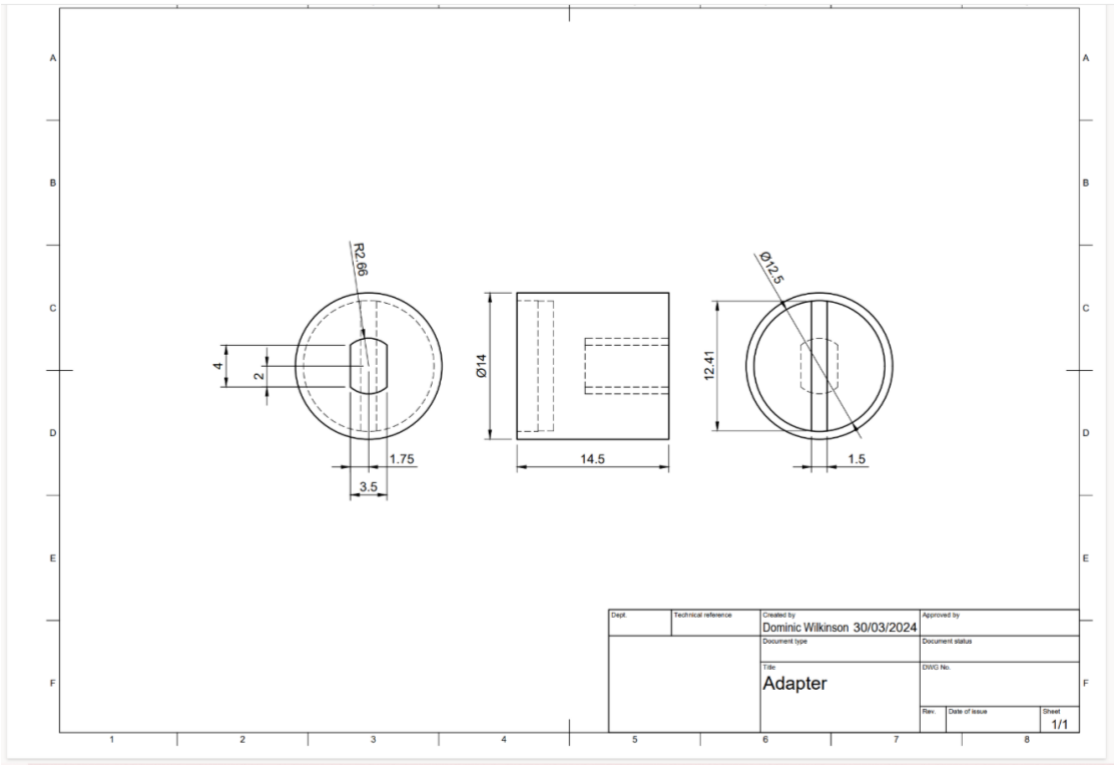

Adapter Version 1

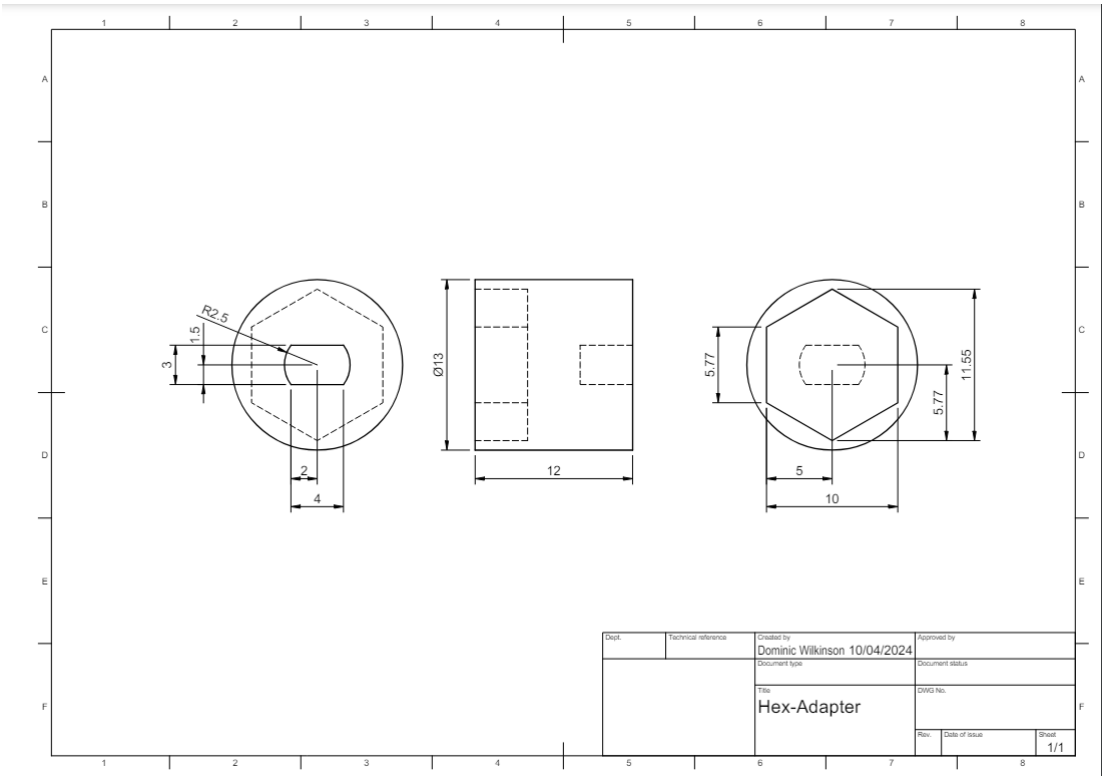

Adapter Final Version

8.5.2 Appendix E.2: Sample Housing

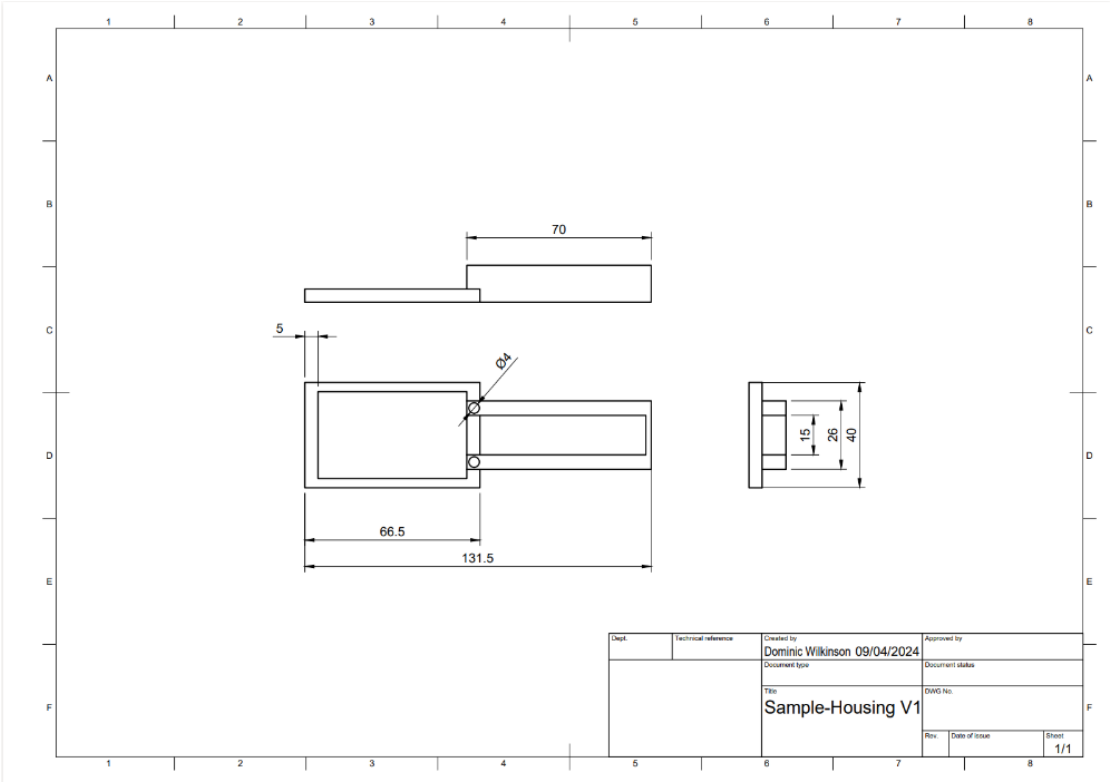

Sample Housing Version 1

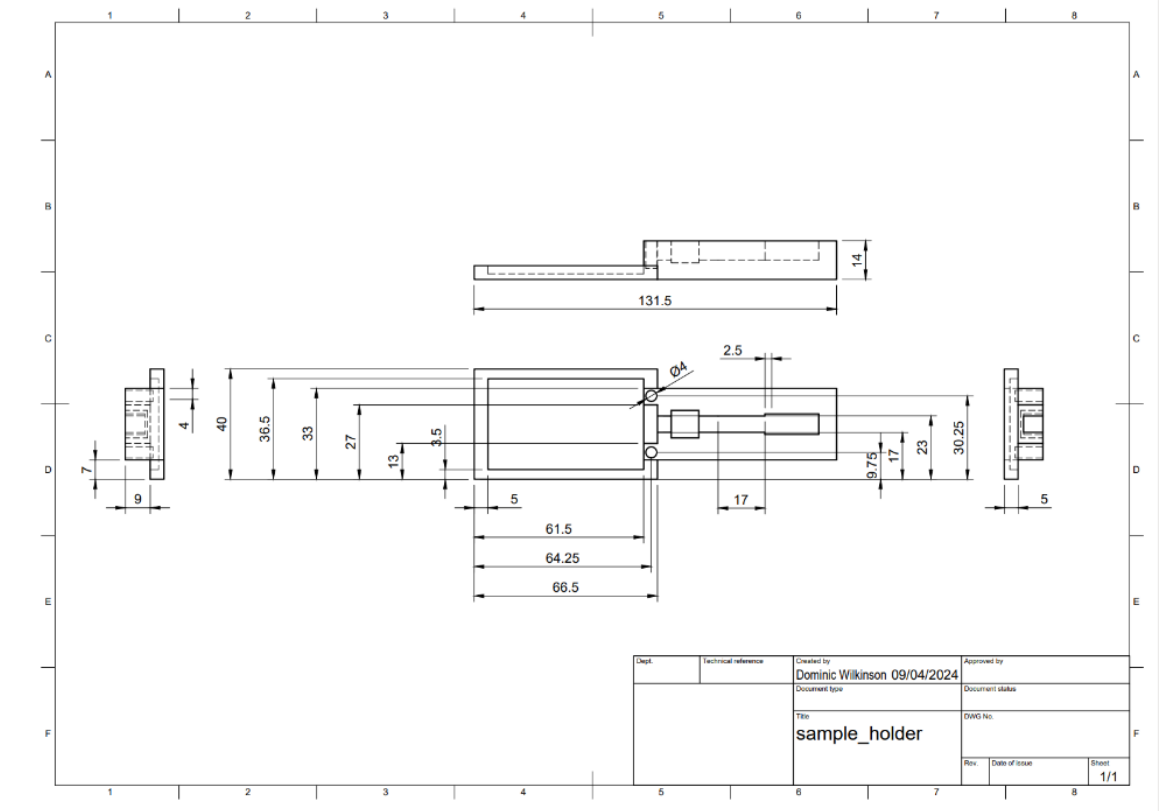

Sample Housing Version 2

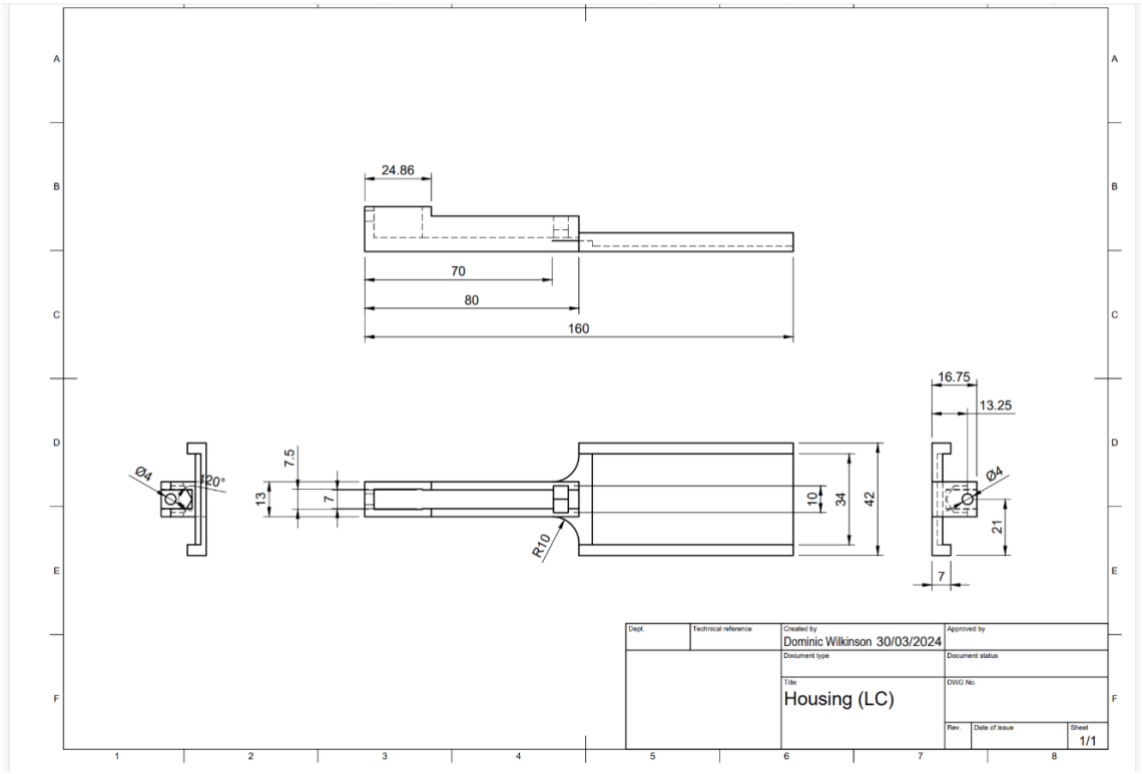

Final Load Cell Housing Design

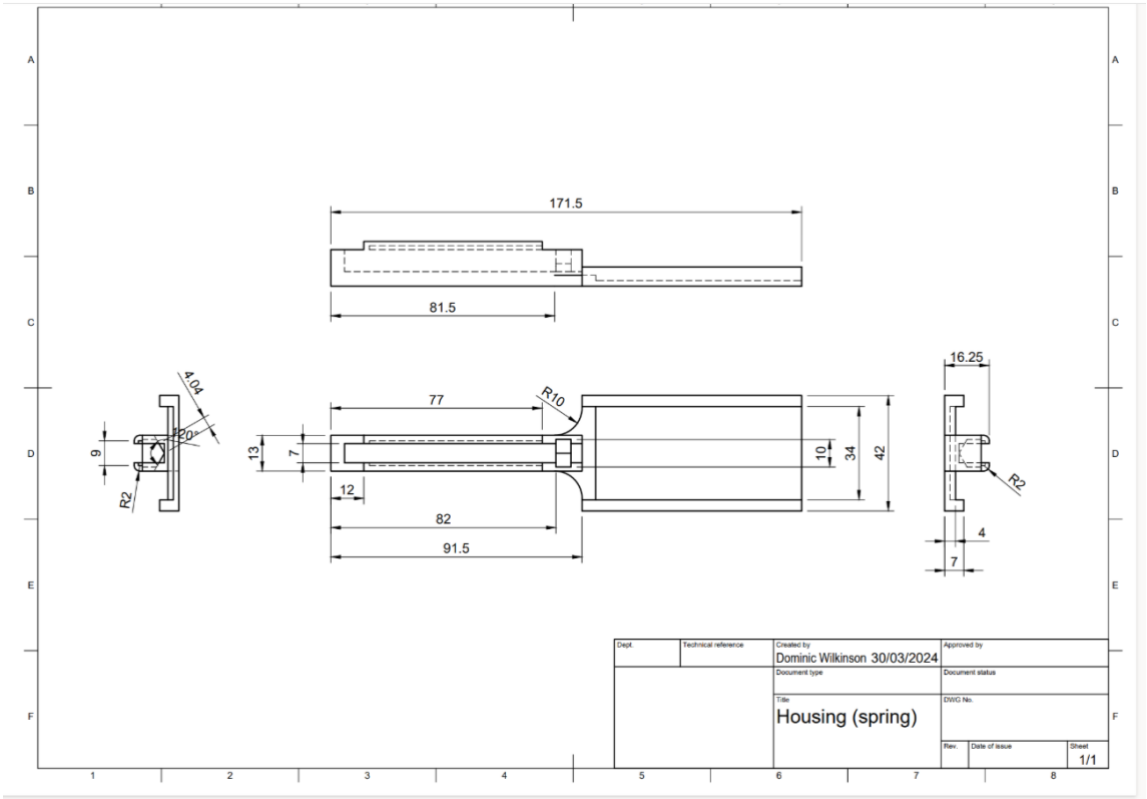

Final Spring Housing Design

8.5.3 Appendix E.3: Motor housing

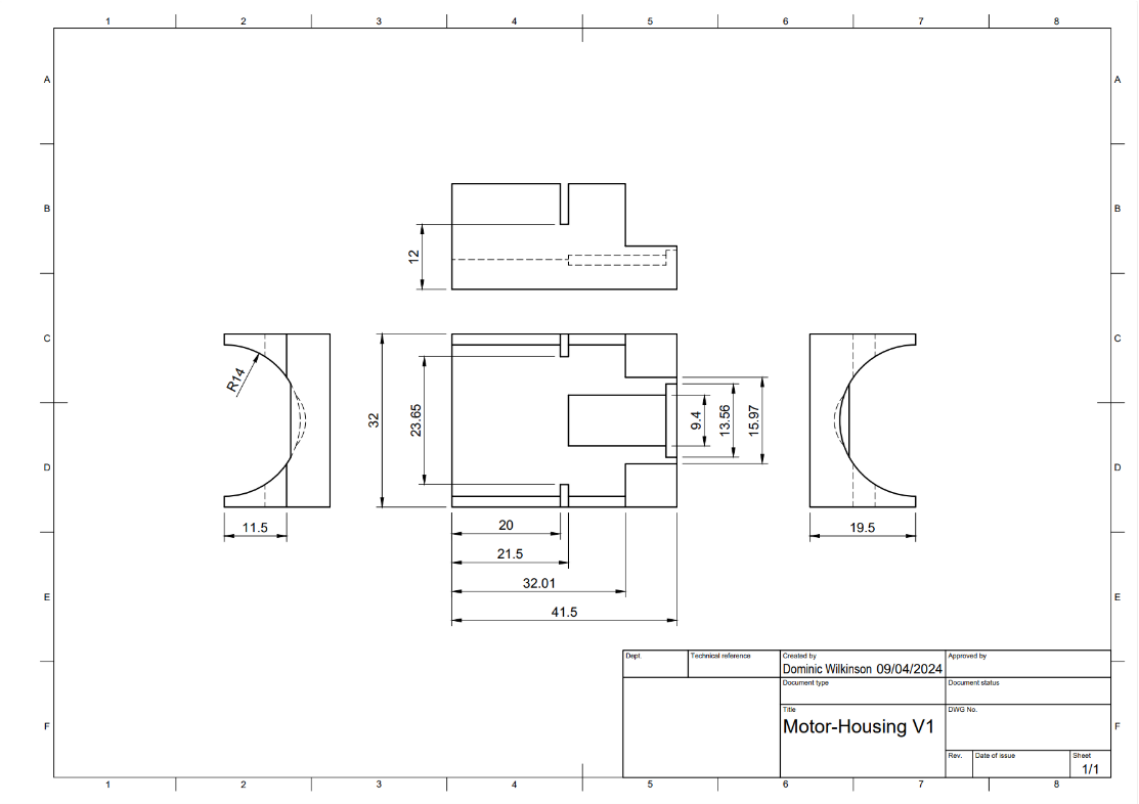

Motor Housing Version 1

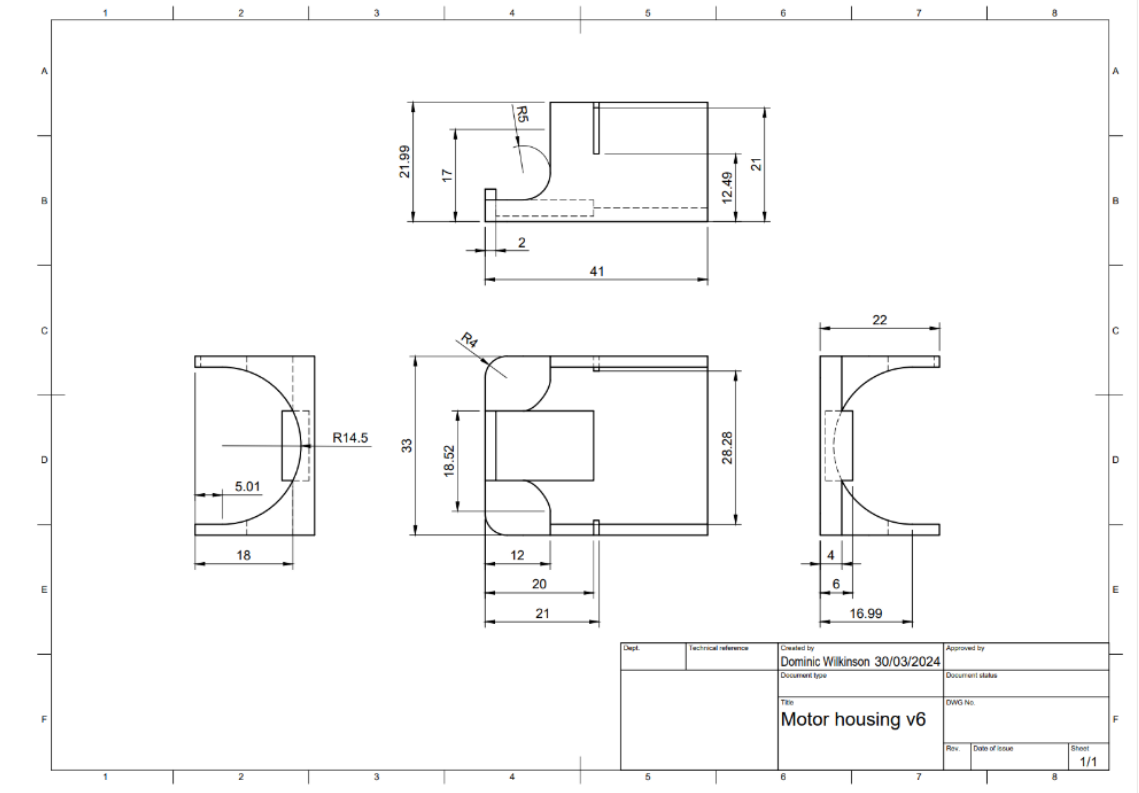

Motor Housing Final Version

8.5.4 Appendix E.4: Voice coil jig

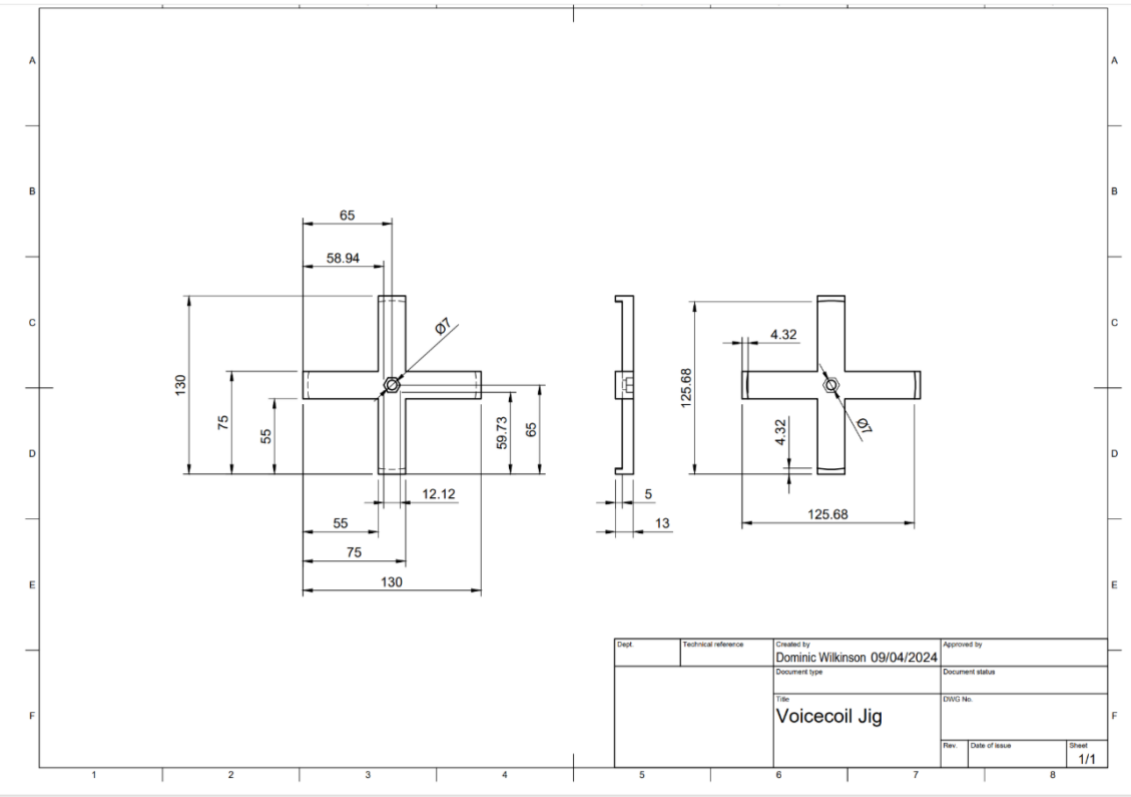

Voice Coil Jig

8.6 Appendix F: DFMEA (Design Failure Modes Effects Analysis)

System/Sub-system	Function	Potential Failure Mode	Potential Failure Effects	SEVERITY (1 - 10)	Potential Causes	OCCURRENCE (1 - 10)	Current Controls	DETECTION (1 - 10)	RPN	Action Recommended
What is the System/Sub-system/Item under investigation	What Function does the System Perform?	In what ways could the System go wrong?	What is the impact on the customer if this failure is not prevented or corrected?		What causes this Failure Mode? (how could it occur?)		What controls exist that either prevent or detect the failure?			What are the recommended actions for reducing the occurrence of the cause or improving detection?
Force Application	**Apply** a known, controlled force to the sample.	Device applies an **inaccurate** force to the sample.	Device cannot perform primary function and cannot be used to obtain accurate data.	10	Calibration error, fault in interface with user, load cell innacuracy.	2	Test individual component accuracy before building device.	8	160	Provide sample material with known properties to check device is accurate validation.
		Device applies force **greater** than user input.	Potential damage to sample and load cell.	7	Unsuitable force application circuit design results in overshoot and steady state error.	8	Modulated step size of force application system to minimise overshoot.	2	112	Implement P controller to minimise steady state error and overshoot.
		Failure of motor	Device cannot perform primary function as it is unable to apply force.	9	Motor overheats or is subject to high humidity due to non-airtight sample housing.	2	Regular monitoring of motor temperature .	5	90	Design protective chamber for motor or utilise moisture pad/agar which won't flow to motor.
		Failure of Arduino	Motor is no longer powered, so force can't be applied. Load cell signal can't be read.	9	Incorrect wiring of arduino e.g. shorting pins or applying voltage to wrong pin.	3	Colour-coded wiring utilised to direct pin connections.	4	108	Produce schematic of pin providing instructions for connection.
		Device applies a **non-uniform** force across the sample.	Cannot **observe** the behaviour specified by the experiment hypothesis.	7	Sample is incorrectly positioned, screw isn't properly held in place, sample doesn't have suitable dimensions.	5	Check orientation of sample prior to force application.	2	70	Add in track pins to ensure force is applied in the right orientation and position. Advise users of suitable sample dimensions.
Tissue Housing Chamber	**Enclose** tissue sample in chamber, in tandem with force application components.	Material failure, chamber breaks.	Sample is lost and device must be reconstructed.	8	Chamber is dropped or hit by heavy object.	2		2	32	Use more robust materials to house tissue.
		Insecure housing (internal components are loose).	Force not properly applied, load cell readings likely inaccurate, sample can slip.	8	3D printing error or design error in CAD.	3	Check the printed chamber before usage.	4	96	Refine tolerances of printing such that a small error does not compromise device.
		Chamber is not watertight.	Risk to motor, sterility of sample is compromised.	6	Design flaw/printer tolerances.	9		3	162	Utilise moisture pad or agar instead of fluid immersion to eliminate risk to components.
Force Measurement	**Quantify** force being applied to sample and incorporate in feedback.	Load Cell is not correctly calibrated.	Invalidates results gathered from experiments and could result in excessive force application.	9	Calibration program not used prior to experiment or calibration load incorrectly measured.	3	Incorporate calibration program in general force application program.	3	81	Provide object with known mass for user calibration.
		Spring buckles	Cannot obtain force applied to sample and risk of microscope slide shattering.	9	Excessive force applied, spring with unsuitable properties chosen.	4	Test device with multiple springs and find most suitable stiffness.	2	72	Incorporate thicker microscope slide and provide suitable spring.
Imaging Using OCT	**Image** the sample, quantifying remodelling over 3-14 days.	Device is **incompatible** with microscopes and OCT.	Compression of sample cannot be imaged.	10	Materials used for housing chamber/hardware or the sample medium have unsuitable optical properties.	3	Use materials and media known to be imaging compatible or test materials under imaging equipment before use.	1	30	Quality control of device - check during manufacture.
		Maintain a **living sample** for 3-14 days.	Sample housing chamber is **not moist** enough and medium can't sustain sample	5	Medium for storing the plant sample isn't moist enough, doesn't cover the sample entirely, or contains insufficient nutrients.	4	Using known live plant sample mediums and test to see if the sample can be sustained.	6	120	Using a standard medium to ensure suitability: dilute agar solution used to sustain the tissue sample.

8.7 Appendix G: Expense Sheet

8.7.1 Appendix G.1: Load cell-based design expense sheet

Item	Purpose	Quantities	Supplier	Price
3D Printed (£1.24)				
Adapter	Connects motor to bolt	1	Printed	£0.05
Motor Housing	Holds motor in place and slides	1	Printed	£0.32
Load Cell Housing	Holds load cell, sample, and motor housing	1	Printed	£0.77
15mm Block	Compress the sample	2	Printed	£0.06
10mm Block	Compress the sample	2	Printed	£0.04
Purchased (£736.15)				
Stepper Motor	Rotates bolt to compress sample	1	RS	£4.74
HX711	Obtains the output of the load cell	1	RS	£11.02
M6 Nut	Converts rotation into linear movement	1	RS	£0.11
M6 Bolt	Used as compressor	1	RS	£0.23
Arduino Nano	Manages feedback and control	1	RS	£11.52
Load Cell	Measures and feedback force applied	1	Logicbus	£708.53
			Total Price:	**£737.39**

8.7.2 Appendix G.2: Spring-based design expense sheet

Item	Purpose	Quantities	Supplier	Price
3D Printed (£1.31)				
Adapter	Connects motor to bolt	1	Printed	£0.05
Motor Housing	Holds motor in place and slides	1	Printed	£0.32
Spring Housing	Holds spring, sample, and motor housing	1	Printed	£0.84
15mm Block	Compress the sample	2	Printed	£0.06
10mm Block	Compress the sample	2	Printed	£0.04
Purchased (£17.85)				
Stepper Motor	Rotates bolt to compress sample	1	RS	£4.74
M6 Nut	Converts rotation into linear movement	1	RS	£0.11
M6 Bolt	Used as compressor	1	RS	£0.23
Arduino Nano	Manages feedback and control	1	RS	£11.52
Spring	Allows calculations of force via displacement	1	RS	£1.25
			Total Price:	**£19.16**

8.8 Appendix H: Key Objective Analysis

Load cell prototype key objective analysis

Objective	Achieved?	Description
Application of a user-specified compressive force or deformation	Yes	▪ Resolution via deformation application mode: 0.49um ▪ Resolution via force application mode: 1mN (load cell model dependent) ▪ Strain/force application rate can be controlled
Application of a sustained force or deformation	Yes	▪ Compression via deformation application mode can be held indefinitely (no power required) ▪ Compression via force application mode can be held until power supply or component fails
Compatibility with non-invasive imaging techniques	Yes	▪ Compatible with OCT's magnified video feed function (comparable with USB light microscopy) ▪ OCT scanning function not suitable for current device setup
Characterisation of global sample mechanical properties	Yes	▪ Force and displacement data recorded throughout compressive, hold & decompressive loading phases
Characterisation of local mechanical properties	Yes	▪ Displacement map generation by using imaging data in tandem with recorded force & displacement data
Characterisation of anatomical changes e.g. pore size	Yes	▪ Pore analysis achievable via imaging data ▪ Characterisation of remodelling ability not tested due to limitations of cellulose sponge
Affordability	Yes	▪ Load cell prototype (£737) significantly cheaper relative to existing devices e.g. Linkam Modular Force Stage (£48000) ▪ Calibrated spring prototype (£19) further enhances affordability
Reusability	Yes	▪ Parts remain constant, samples can be freely exchanged
Low resource intensity	Yes	▪ Minimal parts required ▪ Entire housing can be 3D printed
Sterility & preservation of sample over 14 days	No	▪ Sample chamber not closed with hermetic seal ▪ Screw and blocks move in and out of sample chamber ▪ Nutrient media e.g. agar not compatible with load cell prototype

Calibrated spring prototype key objective analysis

Objective	Achieved?	Description
Application of a user-specified compressive force or deformation	No	▪ Buckling of spring restricted force application to sample
Application of a sustained force or deformation	No	▪ Buckling of spring restricted force application to sample
Compatibility with non-invasive imaging techniques	Yes	▪ Compatible with OCT's magnified video feed function (comparable with USB light microscopy) ▪ OCT scanning function not suitable for current device setup
Characterisation of global sample mechanical properties	No	▪ Not tested due to issues with force application
Characterisation of local mechanical properties	No	▪ Not tested due to issues with force application
Characterisation of anatomical changes e.g. pore size	No	▪ Not tested due to issues with force application
Affordability	Yes	▪ £19 production cost
Reusability	Yes	▪ Parts remain constant, samples can be freely exchanged
Low resource intensity	Yes	▪ Minimal parts required ▪ Entire housing can be 3D printed
Sterility & preservation of sample over 14 days	No	▪ Sample chamber not closed with hermetic seal ▪ Screw and blocks move in and out of sample chamber

8.9 Appendix I: Resolution Calculation

The resolution of the applied displacement is given by:

$$Resolution = \frac{Pitch\ of\ bolt}{Number\ of\ revolutions\ of\ stepper\ motor}$$

The number of revolutions of the stepper motor is 2048 (8.16) and the pitch of an M6 bolt is 1mm.

Thus,

$$Resolution = \frac{1mm}{2048} = 0.000488mm = 0.488\mu m\ (3\ s.f.)$$

8.10 Appendix J: OCT images

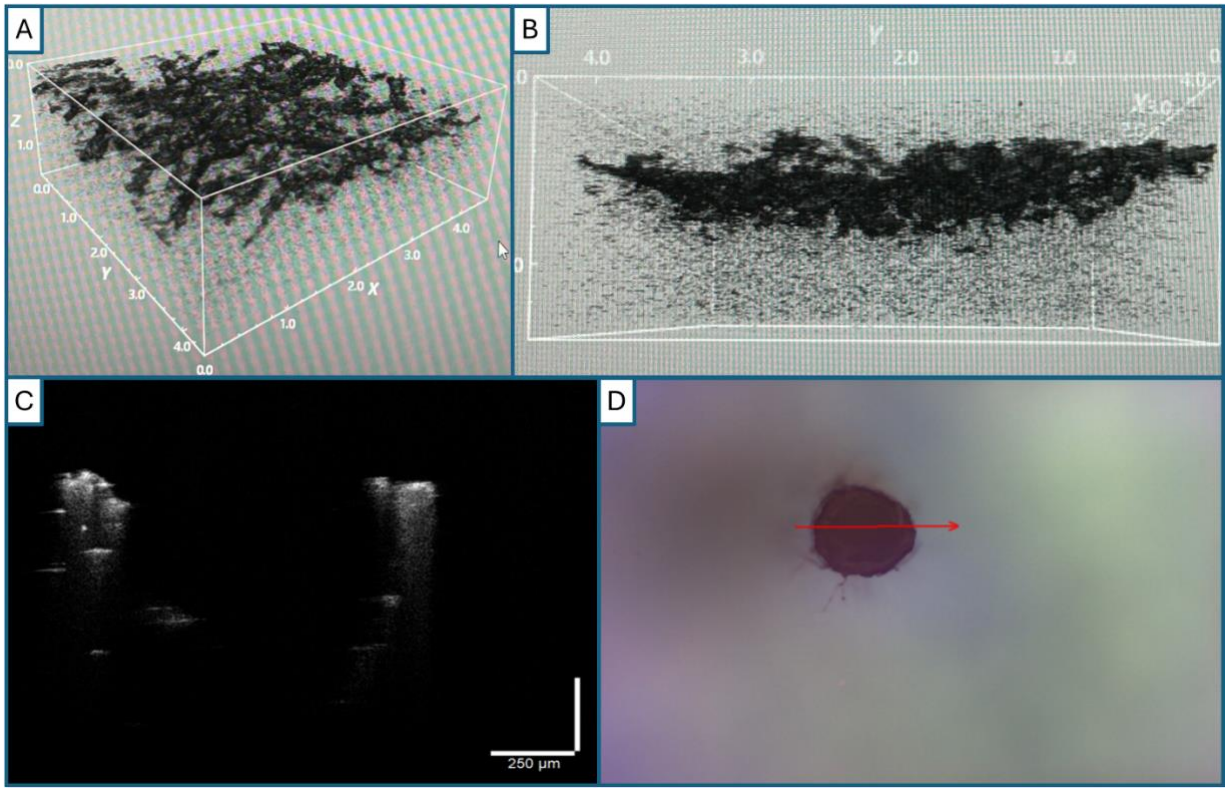

Images showing various scans from the OCT device.

(A&B) - 3D scan of the surface of a sponge sample from two angles. Low resolution can be observed, with poor depth penetration due to backscattering.

(C) Depth scan of plant stem section (D) Video feed image, OCT is scanning through the red arrow. The stem wall on either side can be observed with poor depth penetration. No other structures can be clearly discerned.

8.11 Appendix K: Spring Buckling

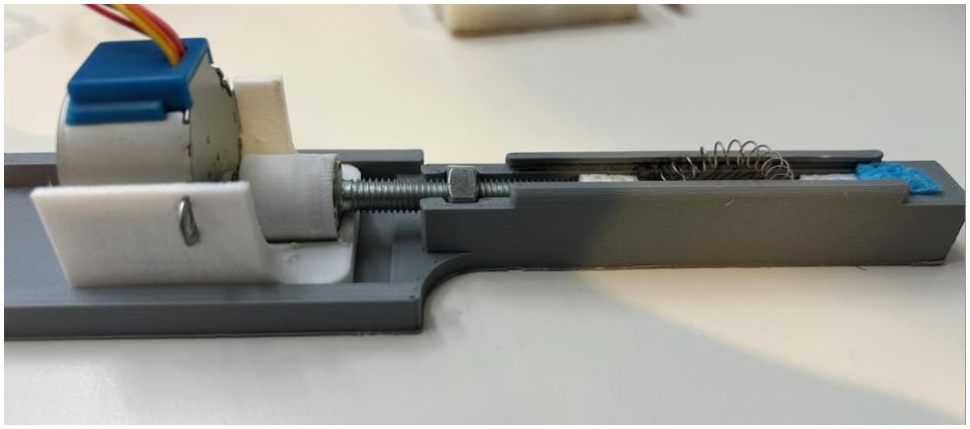

8.12 Appendix L: Github

[BonniciJ/CellULoad (github.com)]

8.13 Appendix M: UI

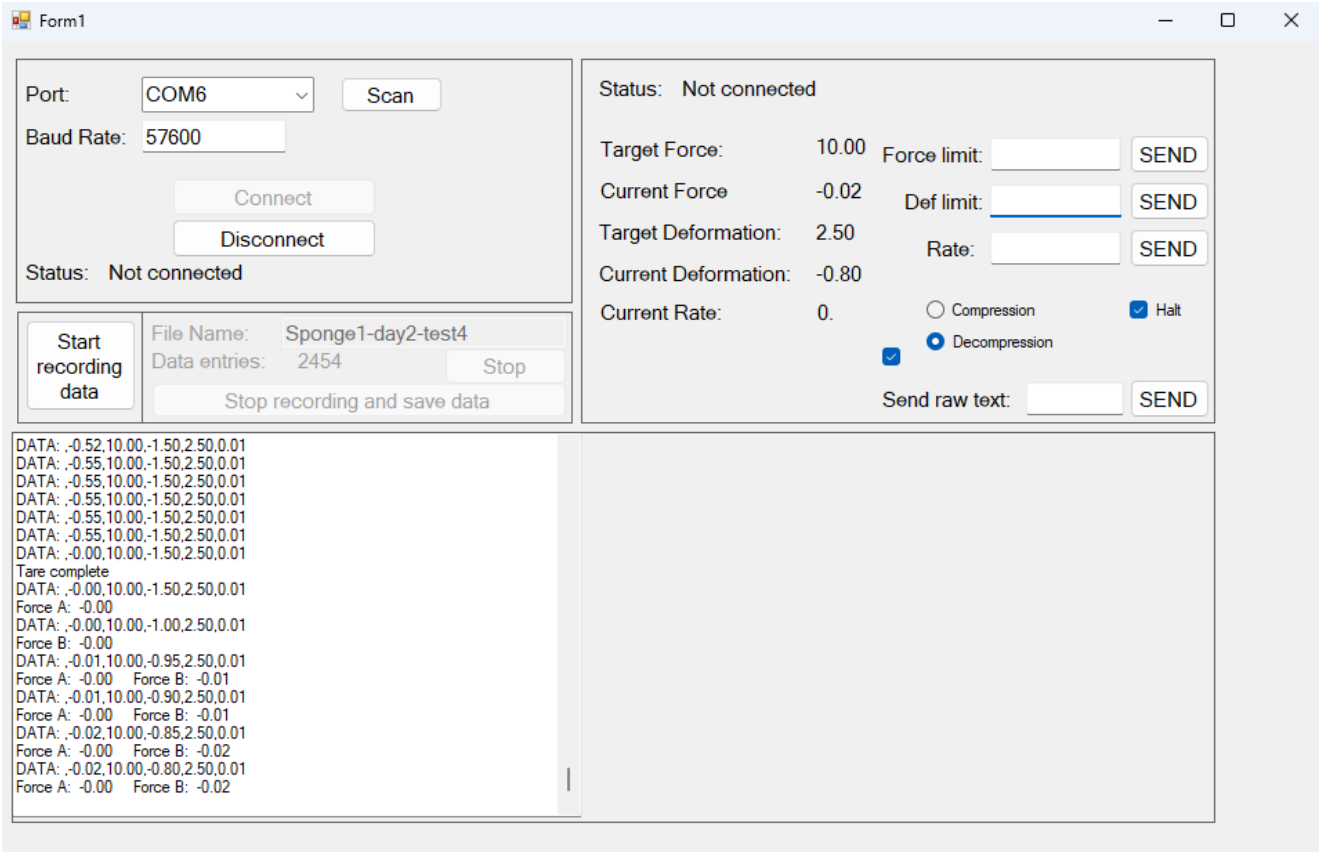

8.14 Appendix N: Pseudo Code

INITIALISE:

Connect to Load Cell

Connect to stepper motor

Unwind stepper motor until there is no change in force reading (i.e. we are fully retracted)

Wind the screw in until a very small force is detected on the load cell (i.e. we are barely touching the sample)

Displacement = 0

Force = 0

APPLY A TARGET FORCE:

targetForce = 10 (e.g. 10. Can be any value between 0-100)

error = currentForce – targetForce

step = *control*(error)

move(step)

Function *control* (error) {

Define the P constant

step = error * P

Could add in functionality for I and D if needed

Return step

}

Function *move* (distanceToMove) {

pitch = 1 pitch of the bolt in mm

stepsPerRevolution = 2048 number of steps per revolution of the stepper motor

stepsToMove = (distanceToMove / pitch) * stepsPerRevolution

steppermotor.move(stepsToMove)

}

Alternatively, measure the force and apply a small, constant step to reach a target displacement, ensuring you stop at a force limit if needed. Add delay to control rate of deformation (considering the time it takes for the motor to turn)

8.15 Appendix O: Arduino Code

```
#include <HX711_ADC.h>
#include <Stepper.h>

void(* resetFunc) (void) = 0;

// initialize the stepper library on pins 8 through 11:
const int stepsPerRevolution = 2048;  // resolution of motor
Stepper myStepper(stepsPerRevolution, 8, 10, 9, 11);

//pins:
const int HX711_dout = 4; //mcu > HX711 dout pin
const int HX711_sck = 3; //mcu > HX711 sck pin

//HX711 constructor:
HX711_ADC LoadCell(HX711_dout, HX711_sck);

unsigned long t = 0;

float targetF = 10;   //target force
float displacement = 0; //current displacement

void setup() {

Serial.begin(57600); delay(10); //start the serial port on a baud rate the load cell can understand

// set the speed at 5 rpm:
myStepper.setSpeed(5);

//Set up the load cell

LoadCell.begin();
//LoadCell.setReverseOutput(); //uncomment to turn a negative output value to positive
float calibrationValue; // calibration value (see example file "Calibration.ino")
calibrationValue = -43311.62; // uncomment this if you want to set the calibration value in the sketch

unsigned long stabilizingtime = 2000; // precisicion right after power-up can be improved by adding a few seconds of stabilizing time
boolean _tare = true; //set this to false if you don't want tare to be performed in the next step
LoadCell.start(stabilizingtime, _tare);
if (LoadCell.getTareTimeoutFlag()) {
Serial.println("Timeout, check MCU>HX711 wiring and pin designations");
while (1);
}
else {
LoadCell.setCalFactor(calibrationValue); // set calibration value (float)
//Serial.println("Startup is complete");
}

initialise();

}

int plotCount = 0;

float timePermm = 2; //in mins
float movementRemaining = 0;
int direction = 1;
bool decomp = 0;
float maxCompression = 2.5; //measured in mm. Maximum compression

bool halted = 1;
bool atMaxCompress = 0;
```

```
45) void loop() {



46) if (halted) {
47) delay(50);
48) float force = measure();
49) } else {


50) if (displacement >= maxCompression &&
    !decomp) {
51) // Do not carry on compressing if we are at
    the max compression
52) atMaxCompress = 1;
53) }


54) if (atMaxCompress) {
55) delay(50);
56) if (displacement < maxCompression |
    decomp) {
        a. atMaxCompress = 0;
57) }
58) float force = measure();
59) } else {
60) //if we arent at max compression and we
    arent halted:


61) float force = measure();


62) if (force != -1000) {  //if there is a force
    measurement


        a. if (decomp) {
        b. //decompressing - this part is
           rough, needs improvement


        c. delay(50);
        d. float step;
        e. float error = targetF - force;
        f. step = 0.001 * (error);
        g. float trueStep = move(step);
        h. } else {
        i. //compressing
        j. doCompression(force);


        k. }
```

```
63) } else {
        a. delay(50);
64) }
65) }
66) }


67) listenToSerial();
68) }


69) void doCompression(float force) {
70) float padding = 0.1; //how close is close
    enough force. allows the motor to jitter
    back and forth less
71) float stepSize = 0.001;
72) float trueStep;
73) if ((targetF - force) > padding) {
74) // we need to compress
75) trueStep = move(stepSize);


76) } else if ((targetF - force) < -padding) {
77) // we need to DEcompress
78) trueStep = move(-stepSize);


79) }


80) //delay to ensure slow compression at
    specified rate
81) int timeDelay =
    timePermm*60000*trueStep; //time to do
    one step
82) timeDelay -= trueStep * 7.5 * 1000;
    //correct for the time it takes to turn the
    motor
83) delay(timeDelay);


84) }


85) float prevError = 0;
86) String incoming; //used for incoming
    messages - might be bad to use string??
87) bool isReading = 0;


88) void listenToSerial(){


89) if (Serial.available() > 0) {
90) char inByte = Serial.read();
```

```
91) if (inByte == 'H') halted = true;
92) if (inByte == 'X') halted = false;
93) if (inByte == 'Y') decomp = true;
94) if (inByte == 'K') decomp = false;
95) if (inByte == '_') resetFunc();
    //compress

96) if (inByte == '~') { //stop reading
97) isReading = 0;

98) // used for setting new force and
    deformation limits and the rate
99) if (incoming.substring(0, 3) == "FOR") {
        a. targetF = incoming.substring(3,
           incoming.length()).toFloat();
100)       }
101)       if (incoming.substring(0, 3) ==
    "DEF") {
        a. maxCompression =
           incoming.substring(3,
           incoming.length()).toFloat();
102)       }
103)       if (incoming.substring(0, 3) ==
    "RAT") {
        a. timePermm =
           incoming.substring(3,
           incoming.length()).toFloat();
104)       }

105)       // //used to change mode
106)       // if (incoming.substring(0, 6) ==
    "DECOMP") { //decompression mode (i.e.
    fast rate)
107)       //   decomp = 1;
108)       // }
109)       // if (incoming.substring(0, 4) ==
    "COMP") { //compression mode (i.e.
    constant, low rate)
110)       //   decomp = 0;
111)       // }

112)       } else if (inByte == '#') { //start
    reading
113)       isReading = 1;
114)       incoming = "";
115)       } else if (isReading) { //read
116)       incoming.concat(inByte);
117)       }
118)       }
119)       }
```

```
120)

121)       float measure() {

122)       float measurement = -1000;

123)       static boolean newDataReady = 0;
124)       const int serialPrintInterval = 10;
    //increase value to slow down serial print
    activity

125)       // check for new data/start next
    conversion:
126)       if (LoadCell.update())
    newDataReady = true;

127)       // get smoothed value from the
    dataset:
128)       if (newDataReady) {
129)       float i;

130)       i = LoadCell.getData();
131)       newDataReady = 0;

132)       measurement = i;

133)       //Plot force
134)       if (plotCount = 1000 && i != -
    1000) {
135)       Serial.println("DATA: ," +
    String(i) + "," + String(targetF) + "," +
    String(displacement) + "," +
    String(maxCompression) + "," +
    String(timePermm));
136)       plotCount = 0;
137)       } else {
138)       plotCount++;
139)       }

140)       }

141)       return measurement;

142)       }
```

```
143)        float move(float dist) {
144)        //postive values compress
145)        //dist is measured in mm
146)        float pitch = 1;
147)        float revolutions = dist / pitch;
148)        int steps = stepsPerRevolution *
    revolutions;

149)        float trueDisplacementChange =
    steps * (pitch / stepsPerRevolution);
150)        displacement +=
    trueDisplacementChange;

151)        myStepper.step(-steps);

152)        return trueDisplacementChange;
153)        }

154)        void initialise() {

155)        //Find the start of the sample - i.e.
    the zero point

156)        //First unload completely
157)        delay(100);
158)        float forceA = -1000;
159)        while (forceA == - 1000) {
160)        forceA = measure();
161)        Serial.print("Force A:  ");
162)        Serial.println(forceA);
163)        }

164)        float trueStep; //just a placeholder
165)        trueStep = move(-1);
166)        delay(1000);
167)        float forceB = measure();
168)        forceB = measure();
169)        forceB = measure();
170)        //Serial.print("Force B:  ");
171)        //Serial.println(forceB);

172)        while (abs(forceA - forceB) > 0.1)
    {
173)        delay(100);
174)        forceA = measure();
175)        trueStep = move(-0.5);
176)        forceB = measure();
177)        Serial.print("Force A:  ");
178)        Serial.print(forceA);
179)        Serial.print("     Force B:  ");
180)        Serial.println(forceB);
181)        }

182)        Serial.println("ZERO -
    UNLOADED");
183)        LoadCell.tareNoDelay();
184)        // wait until last tare operation is
    complete:
185)        bool tared = false;
186)        while (!tared) {
187)        delay(10);
188)        measure();

189)        if (LoadCell.getTareStatus() ==
    true) {
190)        tared = 1;
191)        }
192)        }
193)        Serial.println("Tare complete");

194)        //Next screw in unitl zero point
    (until small increase in load
195)        delay(100);
196)        forceA = -1000;
197)        while (forceA == - 1000) {
198)        forceA = measure();
199)        Serial.print("Force A:  ");
200)        Serial.println(forceA);
201)        }

202)        trueStep = move(0.5);
203)        forceB = measure();
204)        Serial.print("Force B:  ");
205)        Serial.println(forceB);

206)        while (abs(forceA - forceB) < 0.3)
    {
207)        delay(10);
208)        trueStep = move(0.05);
209)        forceB = measure();
210)        Serial.print("Force A:  ");
211)        Serial.print(forceA);
212)        Serial.print("     Force B:  ");
213)        Serial.println(forceB);
214)        }

215)        Serial.println("ZERO
    DISPLACEMENT");
```

```
216)        LoadCell.tareNoDelay();
217)        displacement = 0;


218)        // wait until last tare operation is
    complete:
219)        tared = false;
220)        while (!tared) {
221)        delay(10);
222)        measure();


223)        if (LoadCell.getTareStatus() ==
    true) {
224)        tared = 1;
225)        }
226)        }
227)        Serial.println("Tare complete");
```

8.16 Appendix P: Data Sheets

Stepper Motor (24BYJ48): https://docs.rs-online.com/7206/0900766b8168eba5.pdf

Load Cell Click (HX711): https://docs.rs-online.com/fd72/A700000009001419.pdf

M6 Hex-nut (189-591): https://docs.rs-online.com/ca1a/A700000007925456.pdf

M6 Bolt (190-175): https://docs.rs-online.com/2d77/0900766b8157e8b5.pdf

Arduino Nano (NANOEveryV3.0): https://docs.rs-online.com/1d66/A700000006519064.pdf

Load Cell (LSB200) : https://media.futek.com/content/futek/files/pdf/productdrawings/lsb200.pdf

Spring (121-264): https://docs.rs-online.com/69f5/0900766b8157e218.pdf

OCT Manual: https://www.thorlabs.com/catalogpages/Obsolete/2020/OCTG-900.pdf